

CPD

11, 5549–5604, 2015

ENSO
reconstructions

L. M. K. Henke et al.

Was the Little Ice Age more or less El Niño-like than the Mediaeval Climate Anomaly? Evidence from hydrological and temperature proxy data

L. M. K. Henke¹, F. H. Lambert², and D. J. Charman¹

¹Department of Geography, College of Life and Environmental Sciences, University of Exeter, Amory Building, Rennes Drive, Exeter, EX4 4RJ, UK

²Department of Mathematics, College of Engineering, Mathematics and Physical Sciences, Harrison Building, Streatham Campus, University of Exeter, North Park Road, Exeter, EX4 4QF, UK

Received: 21 October 2015 – Accepted: 13 November 2015 – Published: 26 November 2015

Correspondence to: L. M. K. Henke (lmkh201@exeter.ac.uk)

Published by Copernicus Publications on behalf of the European Geosciences Union.

Title Page

Abstract

Introduction

Conclusions

References

Tables

Figures



Back

Close

Full Screen / Esc

Printer-friendly Version

Interactive Discussion



Abstract

The El Niño–Southern Oscillation (ENSO), an ocean–atmosphere coupled oscillation over the equatorial Pacific, is the most important source of global climate variability on inter-annual time scales. It has substantial environmental and socio-economic consequences such as devastation of South American fish populations and increased forest fires in Indonesia. The instrumental ENSO record is too short for analysing long-term trends and variability, hence proxy data is used to extend the record. However, different proxy sources have produced varying reconstructions of ENSO, with some evidence for a temperature–precipitation divergence in ENSO trends over the past millennium, in particular during the Mediaeval Climate Anomaly (MCA; AD 800–1300) and the Little Ice Age (LIA; AD 1400–1850). This throws into question the stability of the modern ENSO system and its links to the global climate, which has implications for future projections. Here we use a new statistical approach using EOF-based weighting to create two new large-scale ENSO reconstructions derived independently from precipitation proxies and temperature proxies respectively. The method is developed and validated using pseudoproxy experiments that address the effects of proxy dating error, resolution and noise to improve uncertainty estimations. The precipitation ENSO reconstruction displays a significantly more El Niño-like state during the LIA than the MCA, while the temperature reconstruction shows no significant difference. The trends shown in the precipitation ENSO reconstruction are relatively robust to variations in the precipitation EOF pattern. However, the temperature reconstruction suffers significantly from a lack of high-quality, favourably located proxy records, which limits its ability to capture the large-scale ENSO signal. Further expansion of the palaeo-database and improvements to instrumental, satellite and model representations of ENSO are needed to fully resolve the discrepancies found among proxy records.

ENSO reconstructions

L. M. K. Henke et al.

[Title Page](#)

[Abstract](#)

[Introduction](#)

[Conclusions](#)

[References](#)

[Tables](#)

[Figures](#)



[Back](#)

[Close](#)

[Full Screen / Esc](#)

[Printer-friendly Version](#)

[Interactive Discussion](#)



1 Introduction

The El Niño-Southern Oscillation (ENSO) is the most influential source of inter-annual variability in the modern climate. Defined by anomalous sea surface temperatures (SSTs) and surface pressure patterns, it has substantial environmental and socio-economic consequences. For example, the 1997–1998 strong El Niño event caused intense forest and peat fires in Indonesia which led to additional carbon dioxide (CO₂) releases equivalent to 13–40% of the contemporary global annual emissions (Page et al., 2002). It also devastated fisheries along the Pacific coast of South America (cf. Badjeck et al., 2010), has been linked to disease outbreaks (cf. Hjelle and Glass, 2000; Kovats et al., 2003), and caused an estimated 22 000 deaths and costs of over USD 36 billion (Buizer et al., 2000).

It is important to understand the natural range of ENSO variability to determine whether events such as the 1997–98 El Niño are truly “extreme”. Knowledge of inherent ENSO variability is vital for placing the relatively short observed record into a long-term context. It allows for an evaluation of the effects of anthropogenic impacts on recent and future ENSO trends, which is an area of active research (Collins, 2005; Guilyardi et al., 2009; Vecchi and Wittenberg, 2010; Bellenger et al., 2014). Most current global climate models (GCMs) are deficient in their ability to simulate many aspects of the modern day ENSO, often overestimating the western extent of the Pacific Cold Tongue and failing to correctly simulate central Pacific precipitation anomalies, ENSO feedbacks, and ENSO amplitude (Bellenger et al., 2014; Collins, 2005; van Oldenborgh et al., 2005). This translates into uncertainty over their simulations of past (and future) changes in ENSO, calling for alternative sources of climatic information to supplement, complement and corroborate the model and instrumental data. This is done using proxy records such as tree rings, tropical ice cores, sediment cores and corals.

Proxy, instrumental and modelling studies have shown links between ENSO and global and remote regional climate variability on inter-annual (Klein et al., 1999; Wang et al., 1999), decadal (Nelson et al., 2011), centennial (Mann et al., 2005; Trouet

ENSO reconstructions

L. M. K. Henke et al.

Title Page

Abstract

Introduction

Conclusions

References

Tables

Figures



Back

Close

Full Screen / Esc

Printer-friendly Version

Interactive Discussion



et al., 2012) and millennial (Cane, 2005; Ivanochko et al., 2005; Moy et al., 2002; Shin et al., 2006) time-scales. A wide range of proxy records and modelling studies point to substantial changes in ENSO linked to changes in solar variability on orbital time-scales (Clement et al., 2001; Barron and Anderson, 2011), movement of the Intertropical Convergence Zone (ITCZ; Partin et al., 2007; Gomez et al., 2004; Carré et al., 2005; Nelson et al., 2011) and changes in ocean circulation linked to sea level rise (Wanner et al., 2008; McGregor et al., 2008). In the more recent past, changes in solar irradiance and stratospheric aerosol loadings due to volcanic activity have played significant roles in modulating the hemispheric to global scale climate (Mann et al., 2009). The so-called Mediaeval Climate Anomaly (MCA; ca. AD 800–1200) and the Little Ice Age (LIA; ca. AD 1300–1850) were periods of anomalously warm and cool conditions respectively, at least in the Northern Hemisphere if not globally. Proxy evidence for the past 2000 years appears to be more ambiguous regarding ENSO behaviour however. A range of proxies point to a more northerly ITCZ (Haug et al., 2001; Sachs et al., 2009; Tierney et al., 2010) during the MCA, which is characteristic of La Niña-like conditions and is in agreement with warming patterns found in multiproxy reconstructions of hemispheric and global scale temperature (e.g. Mann et al., 2009). Langton et al. (2008) similarly infer a reduction in ENSO activity during the MCA based on ocean basin ventilation changes in Indonesia. Haug et al. (2001) propose a link with climatic processes in the northern mid-latitudes, such as a strengthened AMOC and a more positive NAO (see also Trouet et al., 2009, 2012). In contrast, a Southern Oscillation Index reconstruction based on two proxy records (Yan et al., 2011a) shows an El Niño-like state during the MCA and a La Niña-like LIA. This seems to be supported by a number of other precipitation proxies from the West Pacific (Yan et al., 2011b) and East Pacific (Moy et al., 2002). Other precipitation proxies indicate a highly variable ENSO during the LIA, including two multidecadal droughts in Java (Crausbay et al., 2006), high amplitude rainfall fluctuations in Madagascar (Brook et al., 1999), and three southerly ITCZ excursions (Haug et al., 2001).

**ENSO
reconstructions**

L. M. K. Henke et al.

[Title Page](#)[Abstract](#)[Introduction](#)[Conclusions](#)[References](#)[Tables](#)[Figures](#)[Back](#)[Close](#)[Full Screen / Esc](#)[Printer-friendly Version](#)[Interactive Discussion](#)

**ENSO
reconstructions**

L. M. K. Henke et al.

[Title Page](#)[Abstract](#)[Introduction](#)[Conclusions](#)[References](#)[Tables](#)[Figures](#)[Back](#)[Close](#)[Full Screen / Esc](#)[Printer-friendly Version](#)[Interactive Discussion](#)

These discrepancies in ENSO trends between various proxy records raise two important questions. The current dynamical understanding of ENSO is underpinned by the strong relationship between temperature and rainfall observed in the modern day, and the relationships between the ENSO “source region”, the tropical Pacific, and tele-connected regions, which largely fall between 40° S and 40° N. In light of apparently conflicting stories told by temperature and precipitation proxy records as highlighted by Yan et al. (2011a), the first question is to what extent the modern-day precipitation–temperature relationship in the source and teleconnected regions continues to exist in the past. The second question concerns the relation of ENSO to the wider climate; is there a link between global temperatures and ENSO state on multidecadal to centennial time-scales? A comparison between the MCA and the LIA can give some insight into this, and may hold some clues to what we can expect under anthropogenic climate change.

Hence the use of proxy archives such as corals, tree rings and sediment cores can contribute valuable insights on past climatic events and behaviours by extending the instrumental records back in time, but substantial uncertainties remain. This is because all proxies have inherent limitations and ambiguities that must be identified and dealt with appropriately. These include resolution, dating errors, noise, limited and/or skewed spatial coverage, and nonlinear responses to the climatic variable of interest (Jones et al., 2009). Various statistical techniques have been employed to create multiproxy reconstructions of climatological phenomena, broadly falling into the categories “composite plus scaling” (CPS) or “climate field reconstruction” (CFR) (Jones et al., 2009). CPS encompasses any method which involves combining standardised proxy records into a single reconstruction which is subsequently calibrated to a known timeseries of the target variable (e.g. instrumental temperature record) to provide a quantitative estimate of the variable. CFRs, on the other hand, aim to reconstruct large-scale spatial patterns of climatic change using covariance between proxies and instrumental data. Within both methods there is a wide variety of approaches; see Jones et al. (2009) for

more detailed descriptions and examples of both CPS and a range of CFR methods. The focus of this study calls for a slightly different approach.

Here we create two new ENSO reconstructions – one derived from temperature proxies and one from precipitation proxies – using a new method for assessing the stability of the modern-day ENSO patterns in the source region and the wider tele-connected regions. In a fashion similar to e.g. Braganza et al. (2009), proxy records are not tuned to instrumental data other than a simple location-dependent weighting. While this precludes direct quantitative comparisons, it removes the bias towards high-frequency trends that stems from calibrating to the relatively short (~ 150 year) instrumental record (or indeed any short record; Cook et al., 1995; Jones and Mann, 2004). The method amplifies the ENSO component of proxy records and simultaneously attempts to quantify uncertainty related to noise and incomplete spatio-temporal data coverage, whilst maximising the use of a wide range of tropical proxies. With this, we aim to answer two questions:

1. Do temperature and precipitation proxies show consistent ENSO behaviour over the last millennium?
2. Do the LIA and the MCA differ significantly in their ENSO state?

Section 2 provides a description of the proxy and instrumental/reanalysis data used in this study and a concise overview of the methodology is given in Sect. 3. The results and discussion of the findings are presented in Sects. 4 and 5 respectively before revisiting the research questions and making concluding remarks in Sect. 6.

2 Data description

2.1 Proxy records

For this study, a comprehensive effort was made to collect all published precipitation and temperature records between 40° S–40° N that cover the last 2000 years. The large

ENSO reconstructions

L. M. K. Henke et al.

Title Page

Abstract

Introduction

Conclusions

References

Tables

Figures



Back

Close

Full Screen / Esc

Printer-friendly Version

Interactive Discussion



majority of records were accessed from the NOAA Paleoclimatology and PANGAEA Databases (<https://www.ncdc.noaa.gov/data-access/paleoclimatology-data/datasets>). In addition, over 200 tree ring records were taken from the dataset used by Mann et al. (2008), and hence were subject to their criteria (see Appendix A for details). After collection, all records were screened for a maximum dating error of 60 years. Although somewhat arbitrary, this cut-off was decided by taking double the averaging period of 30 years that is applied to the data prior to analysis. This is a step towards addressing the issue of dating uncertainty while allowing a wider range of proxies to be utilised. Proxies with larger dating errors generally have lower (multi-annual to multi-decadal) resolution but are usually also much longer, and are arguably more useful for capturing long-term trends which may be less evident or reliable in annual-resolution proxies (cf. Cook et al., 1995; Esper et al., 2002; Mann et al., 2008, on low-frequency trends in tree rings). Other quality judgements regarding temporal resolution, record length and proxy location are accounted for by the method explained in Sect. 3 and Appendix B.

2.2 Modern climate datasets

Instrumental climate data are the best available in terms of dating accuracy, calibration and physical basis (Jones and Mann, 2004). However, their spatial coverage is not complete and sharply decreases back in time. The nature of the method used in this study calls for full spatial coverage over a long period; therefore, reanalysis products are more suitable. These are combinations of instrumental and satellite data interpolated using models. The 20th Century Reanalysis Version 2 (20CRv2) is the longest global dataset of atmospheric circulation available, spanning AD 1870–2010. It is based on surface pressure, temperature and sea ice distribution data, filled in with a “deterministic” Ensemble Kalman Filter (EKF). It has a spatial resolution of 2° latitude \times 2° longitude \times 24 vertical pressure levels, and a temporal resolution of up to 6 h. It has been demonstrated that the 20CRv2 is competent at representing the global tropospheric circulation as well as the mean state and variability of the hydroclimate – for a detailed description and evaluation of the product see Compo et al. (2011).

Title Page

Abstract

Introduction

Conclusions

References

Tables

Figures



Back

Close

Full Screen / Esc

Printer-friendly Version

Interactive Discussion



The monthly mean surface air temperature and precipitation rate datasets were downloaded from the NOAA/OAR/ESRL PSD web site (<http://www.esrl.noaa.gov/psd/>).

3 Methodology

The method used in this study combines 20CRv2-derived temperature and precipitation ENSO patterns with a wide range of proxy records to produce two multiproxy ENSO reconstructions: one based on temperature proxies and one based on precipitation proxies. Through the use of so-called pseudoproxy experiments and an array of statistical approaches, it attempts to take into account the effects of proxy selection, the temporal limitations of individual proxies, and non-climatic noise. Firstly, all data were normalised to a mean of zero and a standard deviation of one to account for the real proxy data not being calibrated to the instrumental record. The precipitation and temperature data were normalised over their full period, whereas the proxy data were normalised with respect to a common period for which all have data, which was always at least 100 years (see Sect. 3.1). Empirical Orthogonal Function (EOF) analysis was then performed on the 20CRv2 precipitation and temperature datasets, and the respective EOFs with the strongest ENSO-like patterns were retained (in both cases this was the first EOF). These form the basis for allocating weights to the proxy records.

Pseudoproxies were created using 20CRv2 data timeseries from the real proxy locations, with added white noise to approximate the effects of non-climatic noise in the proxies. The utility of any pseudoproxy exercise lies in the fact that the answer to the question is known, as it can be derived directly from the original model dataset. By putting the “signal plus noise” pseudoproxies through a method to make a reconstruction of the signal, it allows for inferences about the stability and limitations of the method, estimates of uncertainties due to noise and other proxy record characteristics and, as highlighted by this method, it provides a way of objectively and systematically selecting the most appropriate data (see Smerdon, 2012, for a good introduction to pseudoproxy experiments). The proxy records were combined into 1000 “optimal”

CPD

11, 5549–5604, 2015

ENSO reconstructions

L. M. K. Henke et al.

Title Page

Abstract

Introduction

Conclusions

References

Tables

Figures



Back

Close

Full Screen / Esc

Printer-friendly Version

Interactive Discussion



**ENSO
reconstructions**

L. M. K. Henke et al.

[Title Page](#)[Abstract](#)[Introduction](#)[Conclusions](#)[References](#)[Tables](#)[Figures](#)[Back](#)[Close](#)[Full Screen / Esc](#)[Printer-friendly Version](#)[Interactive Discussion](#)

proxy networks using such a pseudoproxy approach to automatically select the best combinations. In each of the 1000 runs the pseudoproxies were “contaminated” by adding different random noise realisations. This approach also acted to filter out proxies whose resolution, length and/or timespan were unfavourable. Each network derived using pseudoproxies was then used to create a real-world ENSO timeseries with associated errors using the real proxy data. The final ENSO reconstruction was taken as the mean of all network timeseries, with an uncertainty envelope determined by the ensemble range and the 5–95th percentile of individual members’ error ranges. A brief overview follows here, with a detailed methodology in Appendix B. The entire process was done separately for precipitation and for temperature.

3.1 ENSO reconstruction

A thousand proxy networks were created via an “add-one-in” pseudoproxy algorithm that automatically builds a network based on which additional proxy improves the reconstructive power of the network the most. Similar to a forward stepwise regression procedure, pseudoproxies are gradually added to a “base” network of zero based on which creates the best new network, until all proxies have been included. The final “optimal” network is that which performed best over all steps. By repeating the process 1000 times adding different random noise series with a signal-to-noise ratio (SNR) of 0.4 each time (Smerdon, 2012), it takes account of variations in ENSO’s influence at different locations and the presence of non-climatic proxy noise to optimally reconstruct the large-scale ENSO pattern. The 20CRv2 dataset from which the pseudoproxies were created was split into a training (1950–2010) and a validation (1871–1949) set. The EOF pattern (which dictates the proxy weights) was derived from only the training data. Pseudoproxies taken from the full (1871–2010) dataset were weighted (“trained”) based on that EOF and networks created accordingly. The ability of these networks to estimate the “true” ENSO timeseries was then established by testing how well the reconstructions tracked the mean over the validation period using the “coefficient of efficiency” score (CE; Eq. B2). Since there is no standard significance test for CE, critical

ENSO reconstructions

L. M. K. Henke et al.

[Title Page](#)

[Abstract](#)

[Introduction](#)

[Conclusions](#)

[References](#)

[Tables](#)

[Figures](#)



[Back](#)

[Close](#)

[Full Screen / Esc](#)

[Printer-friendly Version](#)

[Interactive Discussion](#)



values (CE_{crit}) were calculated for each network by repeating the reconstructions using pure noise series in lieu of the pseudoproxies. If the validation CE failed to exceed CE_{crit} , the network's reconstruction was deemed to be no better than random noise and was consequently discarded.

The remaining networks were used to create an ensemble of real ENSO reconstructions, using the real proxy data. The proxy records were first normalised to account for the different units (Eq. B1; note this and other pre-processing steps were also applied to the pseudoproxies discussed above). All ensemble members (ENSO timeseries derived from the networks) were then re-normalised to the reference period 0–650 yr BP to ensure comparability. The final ENSO reconstruction was taken as the ensemble mean, while the ensemble range serves as part of its uncertainty envelope.

The last step in creating the reconstructions was calculating the final error range. As the proxy availability varies over time, root mean square errors (RMSEs) were calculated for each timestep separately. This was done by calculating the RMSE for a network that only contains the proxies available at that timestep: for reconstruction ensemble network n , the proxies available at time t were used as a “frozen” (unchanging) network to create 1000 pseudo-reconstructions from which RMSE values were calculated for time t . Repeated for each timestep, this resulted in 1000 absolute error value timeseries for each network n . This was translated into ensemble member uncertainty limits by adding and subtracting the 1000 error series from the ENSO timeseries (to get the maximum and minimum error limits respectively) and taking the 5–95th percentile over their full range. The uncertainty envelope around the final ENSO reconstruction (i.e. the ensemble mean) is thus a combination of the reconstruction ensemble range and the error ranges for individual ensemble members.

While the pseudoproxy experiments described above give some information about the quality of the reconstructions in an ideal world (albeit with random noise), they cannot guarantee the quality of the real proxies. To test this, a “leave-one-out” (LOO) test was performed. It compares the correlation between a single proxy and the ENSO reconstruction made without that proxy in the real world and in an ideal world (again

**ENSO
reconstructions**

L. M. K. Henke et al.

[Title Page](#)[Abstract](#)[Introduction](#)[Conclusions](#)[References](#)[Tables](#)[Figures](#)[Back](#)[Close](#)[Full Screen / Esc](#)[Printer-friendly Version](#)[Interactive Discussion](#)

using pseudoproxies). If the expected (based on pseudoproxies) and observed (from the real proxies) correlations are very different (e.g. opposing signs), it calls for some caution in interpreting the reconstructions and/or using the proxy data. Issues with individual proxies could include systematic (non-random) non-ENSO signals linked to other climatic phenomena such as monsoons, biological processes (e.g. age-related changes in growth rates), or the non-climatic random noise may be higher than estimated (SNR > 0.4) such that the ENSO signal is weaker than simulated by the pseudoproxy. The probability of a lower-than-predicted ENSO signal increases with sparser $n - 1$ networks (the definition of “too sparse” is very subjective, but see e.g. Mann et al., 2007, 2008; Tingley et al., 2012; Wang et al., 2014, for some discussion on the effect of network sparsity on various statistical methods). Alternatively, it could be speculated that the ENSO reconstruction made without the excluded proxy record is inaccurate. For example, at least one of the included proxies may not behave as expected. In this case, those proxies would presumably also show up with unexpected correlations. With so many possible causes for the different correlations, it is difficult to reject any one proxy outright. Instead, some degree of uncertainty must be accepted as proxy data will never be perfect. The impact of said proxies is checked by leaving them out of the network ensemble altogether and comparing this reduced reconstruction with the full version.

The combination of the validation methods and error estimates described here account for a range of uncertainty sources. The add-one-in approach and CE_{crit} threshold measure the expected (pseudo-world) ability of the proxy networks to reconstruct ENSO, while RMSE estimation explicitly takes into account the effect of the estimated proxy noise (which is also addressed by the add-one-in approach through network selection). The LOO test finally inspects the actual performance of the real proxies compared to their expected behaviour, providing a measure of confidence in how realistic the pseudoproxy experiments are, as well as serving as a check on the appropriateness of the real proxies.

3.2 LIA–MCA difference analysis

The absence of a known reference period to which the reconstructions can be calibrated precludes any absolute comparison of the result with recent trends. However, it is possible to ascertain whether the MCA and the LIA differ significantly in how “El Niño-like” they are. Evaluating the LIA–MCA difference directly also removes the bias introduced by taking any reference period (Mann et al., 2009). To do this, the means over the two periods were taken and the MCA mean subtracted from the LIA mean. If the difference is significantly greater than zero, the LIA is more El Niño like than the MCA; if the difference is significantly less than zero, the MCA is more El Niño-like than the LIA.

4 Results: ENSO reconstructions

The final ENSO reconstructions for precipitation and temperature and their proxy network density are shown in Fig. 1. The final number of networks included in the precipitation ensemble is 569, of which 274 are unique (Fig. 1a). The total number of proxies used is 23, with a maximum of 22 for a single network. Proxy availability increases steadily throughout time, save a slight drop off in the most recent period (Fig. 1b). Although there is some spread in the ensemble, particularly in the earliest period, there is a coherent trend visible. The within-ensemble coherence was tested by correlating 1000 randomly chosen pairs with each other. This confirmed that there is generally good agreement over the full period (0–1500 yr BP) as well as during the MCA and LIA individually, with only a few negatively correlated ensemble members during the MCA (Fig. 2). There is a long-term trend towards more ENSO-like conditions evident in the precipitation reconstruction with a slowdown during the MCA.

The temperature reconstruction ensemble consists of 354 optimal networks, all of which are unique (Fig. 1c). The within-ensemble correlations are much lower than for precipitation though still mostly positive, and there is no distinct trend visible in the re-

CPD

11, 5549–5604, 2015

ENSO
reconstructions

L. M. K. Henke et al.

Title Page

Abstract

Introduction

Conclusions

References

Tables

Figures

◀

▶

◀

▶

Back

Close

Full Screen / Esc

Printer-friendly Version

Interactive Discussion



**ENSO
reconstructions**

L. M. K. Henke et al.

[Title Page](#)[Abstract](#)[Introduction](#)[Conclusions](#)[References](#)[Tables](#)[Figures](#)[Back](#)[Close](#)[Full Screen / Esc](#)[Printer-friendly Version](#)[Interactive Discussion](#)

construction. The median proxy coverage (Fig. 1d black line) is worse compared to the precipitation reconstruction; while over half the years in the precipitation reconstruction are based on a median of 11 or more proxies, this value is only 5.5 for temperature. This is despite the significantly higher number of available temperature proxies. However, most of these proxies are tree ring series, all but a handful of which are less than 600 years long (cf. Mann et al., 2008) which is reflected in the steep increase in Fig. 1d, and the vast majority are clustered in North America. This limits the ability of the proxies to cancel out each other's noise and amplify their common ENSO signals, hence diminishing the quality of the reconstruction. The uncertainty range on the temperature reconstruction accordingly increases back in time, much more so than the precipitation reconstruction which shows a relatively consistent uncertainty band (note the different y scales for the two reconstructions). Nevertheless, in both cases the error from proxy noise is overshadowed by the uncertainty associated with the choice of network – the ensemble spread makes up the bulk of the uncertainty envelope.

Figure 3 shows the proxy locations plotted onto the precipitation (top) and temperature (bottom) EOF patterns. The size of the bubbles is an indication how many ensemble members contain the proxy, their colour is the relative EOF weighting with a darker shade being a stronger weighting. The proxies included in the precipitation ensemble members are well-distributed over the western and eastern side of the Pacific. The relatively uniform size of the bubbles suggests that there is no immediate preference of any one proxy over the others.

The spatial distribution of the temperature proxy locations, in contrast, is highly skewed towards North America (Fig. 3), where most of the tree ring records are located. Although a wider range of proxies was considered initially including several in the western and central equatorial Pacific, these were rejected for various reasons including resolution, dating error, length, or low ability to capture the large-scale EOF pattern (see Appendix A and Tables 1 and 2). The combination of this poor spatial coverage, low temporal coverage (Fig. 1d) and wide uncertainty envelope leads to the expectation that the temperature reconstruction is of significantly lower quality than the

precipitation reconstruction. This is indeed supported by the higher error range in the temperature reconstruction.

These maps illustrate the benefit of using the pseudoproxy approach in creating the “optimal” networks. There is no direct correlation between proxy weighting (indicated by the bubble colour) and frequency of use, suggesting that other aspects such as resolution, length and the relationship to other proxy locations played a significant role in determining the usefulness of a proxy which would be difficult to judge from the outset. The fact that the choice of proxy network is the dominant source of error (Fig. 1a and c) is further evidence of the utility of the pseudoproxy “optimal” network method. The high clustering of temperature tree ring records in North America is an example of where the add-one-in method has worked to reduce the risk that some co-varying, non-white noise in a subset of the proxies skews the resulting reconstruction; testing showed that when all North American tree ring records were added to the reconstruction, a regional non-ENSO trend obscured the ENSO signal (not shown).

4.1 Comparing precipitation and temperature

Figure 4 shows the range of LIA–MCA differences for the individual members within the precipitation and temperature ensembles respectively. In the former case, the LIA is significantly more El Niño-like than the MCA ($p < 0.01$). The temperature case is not clear, with the median difference falling on the zero line. The range is also much larger, again reflecting the high uncertainty on the temperature reconstruction.

Figure 5 shows the correlation between 1000 randomly chosen combinations of temperature and precipitation ensemble members as an indication of the agreement between the two climate variables. The agreement is poor, with median correlations close to zero for all years as well as the MCA and the LIA individually. This is most likely a reflection of the high uncertainty on the temperature reconstruction. Therefore, it is not possible to determine a systematic difference between the ENSO signals in temperature and precipitation proxies.

CPD

11, 5549–5604, 2015

ENSO
reconstructions

L. M. K. Henke et al.

Title Page

Abstract

Introduction

Conclusions

References

Tables

Figures



Back

Close

Full Screen / Esc

Printer-friendly Version

Interactive Discussion



4.2 Leave-one-out results

The LOO test results are shown in Fig. 6. Perfectly predicted proxies would fall on the 1 : 1 line, with the most undesirable results in the top-left and bottom-right quadrants (where pseudoproxy and real proxy have opposing signs). As there is random noise in the pseudoproxies (and in addition the noise profiles in real proxies are likely to be more complex than assumed in the proxy experiments), it can be expected that their correlations with the ENSO reconstructions will differ from the pseudoproxy case to some degree. The LOO results are difficult to interpret, and there are no obvious trends. For both temperature and precipitation, real proxy correlations tend to be weaker than pseudoproxy correlations. There is no consistent relationship with proxy type (not shown) or EOF weighting (greyscale shading in Fig. 6). However, there appears to be some link to proxy length particularly in temperature, with shorter proxy records more likely to perform poorly (dot size in Fig. 6). The short proxies in this case tend to be tree rings located in North America, so it is likely that this is a combination of length and location. It is possible that there is some covariability among these records that is not related to ENSO, obscuring the ENSO signal here. Moreover, it could be an expression of the “segment length curse” where the ability of tree rings to capture low-frequency signals is limited by their length (Cook et al., 1995). The two short temperature records with positive pseudoproxy correlations and negative real proxy correlations (bottom right quadrant), incidentally, are both coral records located in the southern West Pacific and are thus subject to different processes that can obfuscate the ENSO signal. Without more detailed analysis (and a larger sample size) it is impossible to make any statistically sound statements regarding these differences however.

As none of the temperature proxies in the anti-correlated quadrants (top-left and bottom-right) are identifiable for having a particularly high correlation in the real world, a “blanket exclusion” of all proxies in those two quadrants was performed to test their influence on the ENSO reconstruction (this is also possible to do in the temperature case as there is a sufficient number of remaining proxies). Despite removing 69 proxies,

CPD

11, 5549–5604, 2015

ENSO
reconstructions

L. M. K. Henke et al.

Title Page

Abstract

Introduction

Conclusions

References

Tables

Figures



Back

Close

Full Screen / Esc

Printer-friendly Version

Interactive Discussion



the reconstruction was not significantly affected with no statistically significant change in the MCA–LIA difference (not shown).

In the case of precipitation, two proxies have a strong positive correlations where a negative correlation is expected (top left quadrant) and one has a strong negative correlation where a positive correlation was expected (bottom right quadrant). Re-creating the reconstruction ensemble excluding these proxies from all networks completely again did not significantly change the final ENSO ensemble, though it did slightly increase the LIA–MCA difference (not shown).

5 Discussion

An important question addressed in this study is whether the modern-day links between temperature and precipitation in ENSO persist back in time. The two ENSO reconstructions presented here provide no strong evidence of a disagreement over whether the LIA or the MCA was more El Niño-like. The precipitation reconstruction suggests the LIA is significantly more El Niño-like than the MCA. The difference between the two periods in the temperature reconstruction is consistent with zero, but very uncertain. The disappointing quality of the temperature reconstruction, which limits the statistical robustness of the precipitation–temperature comparison, is likely due to the low number and unequal distribution of available data locations. Most temperature proxies are located in teleconnected regions outside the ENSO source region, which have been shown to be subject to more temporal variability in precipitation–temperature relationships (Wilson et al., 2010; Coats et al., 2013; Gallant et al., 2013; Lewis and LeGrande, 2015).

Despite the shortcomings of GCMs in simulating the dynamics of ENSO, they are useful for assessing the coupling between equatorial Pacific SST change and impacts on global precipitation and temperature. To test the robustness of this coupling in models, we calculated the correlation between the temperature and precipitation EOF timeseries (PCs) in five GCMs from the Coupled Model Intercomparison Project

Title Page

Abstract

Introduction

Conclusions

References

Tables

Figures



Back

Close

Full Screen / Esc

Printer-friendly Version

Interactive Discussion



ENSO reconstructions

L. M. K. Henke et al.

Title Page

Abstract

Introduction

Conclusions

References

Tables

Figures



Back

Close

Full Screen / Esc

Printer-friendly Version

Interactive Discussion



Phase 5 (CMIP5). All five show a consistently positive correlation over the study region (40° S–40° N) for the historical (AD 1850–2005) and last millennium (AD 850–1850) runs for both annual and 30 year resolution ($R^2 \geq 0.76$, not shown). This is similar to the 20CRv2 data ($R^2 = 0.87$). Understanding and resolving this potential divergence in precipitation and temperature proxy data is thus interesting from a physical dynamical point of view as it contradicts the conventional understanding of ENSO.

There are few other published ENSO-related multiproxy reconstructions based solely on precipitation proxies; these include Stahle et al. (1998) and Yan et al. (2011a), which both focus on the Southern Oscillation Index (SOI, which is negatively correlated with ENSO). Stahle et al. (1998) use a network of tree rings to reconstruct winter SOI between AD 1706–1977. They note a slight tendency towards a stronger mean SOI (i.e. more La Niña-like state) in the latter part of the record, accompanied by increased variability. As this record only covers a fraction of the reconstruction presented in this paper and is focused on annual variability rather than (multi-)decadal trends we cannot draw conclusions about their similarity. A longer (2000 year) record is produced by Yan et al. (2011a), who create a proxy SOI using two precipitation proxies from the Galápagos (Conroy et al., 2008) and the Indo-Pacific Warm Pool (Oppo et al., 2009). Interestingly, the broad trends in their reconstruction are opposite to ours, with a more La Niña-like LIA compared to the MCA. While the two proxies used were considered for this study, they were both rejected due to high dating errors (average around 100 years). Several other precipitation (Tierney et al., 2010; Yan et al., 2011b) as well as temperature (Conroy et al., 2010) proxies supporting the above study's conclusions similarly have high dating errors. Additionally, a reconstruction based on only two proxies is more vulnerable to spurious noise or other climatic influences distorting the ENSO signal, as is evidenced by the degradation back in time of the reconstructions presented in this study as the number of proxies declines.

Most published temperature reconstructions of ENSO focus on one of the NINO regions. A NINO3 region (90–150° W and 5° S–5° N) temperature reconstruction by Mann et al. (2009) shows a slow millennial-scale warming trend (to a more El Niño-like state)

ENSO reconstructions

L. M. K. Henke et al.

Title Page

Abstract

Introduction

Conclusions

References

Tables

Figures



Back

Close

Full Screen / Esc

Printer-friendly Version

Interactive Discussion



from AD 1100 onwards, with relative cooling during the MCA compared to the LIA consistent with a La Niña-like state during the MCA. In contrast, Emile-Geay et al. (2013b) are unable to detect a systematic difference between the MCA and LIA in their Boreal winter NINO3.4 (120–170° W and 5° S–5° N) SST reconstruction. This discrepancy may be due to the difference in proxy networks, particularly the use of lower-resolution proxies here and by Mann et al. (2009) which contribute a substantial part of the signal, or due to the slightly different definition of the NINO regions. In addition to SOI and NINO-region reconstructions, there have been several attempts at reconstructing the coupled ocean–atmosphere ENSO trends and variability (Gergis and Fowler, 2006; Braganza et al., 2009; Gergis and Fowler, 2009; McGregor et al., 2010). However, these are shorter (going back to AD 1500) thus precluding any comparison with the MCA.

A number of other (non-temperature or precipitation) ENSO-sensitive proxies that were not included in our reconstructions support the LIA–MCA difference evident in our reconstruction, although there is less agreement over the mean state of the LIA. Sedimentary sterol concentrations in marine sediment off the Peru coast Makou et al. (2010), suggest the MCA coincides with a reduction in El Niño activity, with both El Niño and La Niña activity increasing from the late MCA onwards. Based on a range of North American proxies Graham et al. (2007) conclude that the MCA was characterised by arid conditions in western North America consistent with a La Niña-like state, followed by a wetter LIA. A basin ventilation record from the Western Pacific Warm Pool (WPWP) (Langton et al., 2008) agrees particularly well with the earlier part of our precipitation reconstruction. It shows a peak in El Niño activity at 1150 yr BP and a distinctive minimum during the MCA, followed by a more El Niño-like LIA characterised by a steady decline in activity. This decline is not apparent in our reconstruction, but is reflected in some other multi-millennial proxy records (Moy et al., 2002; Stott et al., 2004; Conroy et al., 2008).

A multi-region tree ring reconstruction of ENSO variability displays substantial variability in the strength of ENSO teleconnections over time and space (Li et al., 2013). The authors find that the Pacific Northwest and Texas–Mexican regions show highly

**ENSO
reconstructions**

L. M. K. Henke et al.

[Title Page](#)[Abstract](#)[Introduction](#)[Conclusions](#)[References](#)[Tables](#)[Figures](#)[Back](#)[Close](#)[Full Screen / Esc](#)[Printer-friendly Version](#)[Interactive Discussion](#)

unstable teleconnections. This may explain the lack of ENSO signal in the temperature reconstruction presented here, as many of the temperature proxies are located in these regions. If the strength of the teleconnection has changed over time, the weightings based on modern-day ENSO patterns would not reflect this and we would thus lose some ENSO signal. Without proxies located in the centre of action or more robustly teleconnected areas, this loss of signal can be expected to be substantial as suggested by the results here.

An interesting observation of the EOF maps presented here (Fig. 3) is a distinct lack of correlation between EOF weighting and how often proxies are used in a network. Two explanations for this are (i) the climatic noise in the high-occurrence but low-weighted areas is less spatially correlated with the noise elsewhere than in the low-occurrence but higher weighted areas; or (ii) the length and resolution of the proxy records have a more important effect on a proxy's utility than its weighting. The precipitation proxies' frequency of use lends support to the former explanation, as they are all more or less selected a similar number of times regardless of proxy record length or resolution. The latter explanation finds support in the temperature proxy distribution, where several low-weighted but long tree rings (e.g. ca051; Table 2) in North America are strongly preferred by the networks. The reality is probably a combination of both these factors, modulated by the number of proxies available. More detailed analysis will be needed to elucidate this.

5.1 Reflections on the method

The method set out in this study is one of few which attempt to take into account the effect of real spatial and temporal patterns of proxy records, thus increasing our confidence in their ability to accurately evaluate the effectiveness of the networks. To our knowledge, this is the first time that realistic temporal proxy resolution has also been taken into account by the pseudoproxies, in addition to their length (Emile-Geay et al., 2013a; Wang et al., 2014).

ENSO reconstructions

L. M. K. Henke et al.

Title Page

Abstract

Introduction

Conclusions

References

Tables

Figures



Back

Close

Full Screen / Esc

Printer-friendly Version

Interactive Discussion



However, the “optimal” network creation still has scope for improvement. Although we have screened for maximum dating errors, its effect on the included proxies is not explicitly included. This is an issue often neglected in (multi) proxy reconstructions (but see Comboul et al., 2014, for a recent effort to address it systematically). Moreover, our noise simulation is relatively simplistic; the use of a wider noise spectrum (including red, and possibly even blue, noise) may alter the composition of the networks (Smerdon, 2012, and references therein). However, the issue remains that there is no easy way to determine the real noise spectrum of the proxies. Further improvement could come from more accurate estimations of the proxy–climate relationships via proxy system models (e.g. Conroy et al., 2008; Evans et al., 2013; Russon et al., 2013; Stansell et al., 2013; Steinman et al., 2012; Sturm et al., 2010; Thompson et al., 2011; Tierney et al., 2011).

The choice of dataset from which to derive an EOF is also a source of uncertainty (cf. Emile-Geay et al., 2013b), as differences in the EOF pattern will affect the weighting of the proxies. This is pertinent for the precipitation reconstruction, as the modern-day ENSO precipitation signature is much less well-established than for temperature due to less and lower quality data. To test the sensitivity of the results to the choice of dataset, we repeated the precipitation ENSO reconstruction using the Global Precipitation Climatology Project dataset (a combination of surface-based rain gauge data and satellite-derived estimates covering 1979–2012; <http://precip.gsfc.nasa.gov/>). Note that since the dataset is much shorter (AD 1979–2010), it was not possible to divide it into a validation and a training set; instead, the entire dataset was used for both instances. This is the main reason this dataset was not used for the main analysis despite its arguably better representation of the precipitation ENSO pattern. Most importantly, the GPCP–based ENSO reconstruction also shows a significantly more El Niño-like LIA compared to the MCA. Although there were some differences in the EOF pattern of GPCP and 20CRv2, the final ENSO reconstructions showed very similar short-term trends (not shown). The long-term positive trend evident in the 20CRv2-

based reconstruction was not present, however. This is most likely due to divergences in the prevalence of the proxies in the final ensemble.

In addition to the choice of modern dataset, another concern is temporal non-stationarity of EOF patterns within a single dataset. This has been shown to exist in 20CRv2 for the NAO and Pacific North American (PNA), for example, by Raible et al. (2014). We tested the stability of the 20CRv2 temperature EOF used in this study by recalculating it for a running 30 year window and found substantial variability in the spatial pattern and amount of variance captured by the EOF. Further investigation is necessary to explore whether this result is an artefact of internal variability, is due to uncertainties in the reanalysis dataset, or reflects real changes in the nature of ENSO. Nevertheless, it highlights the vulnerability of the majority of ENSO reconstructions (including ours) to the assumption that the modern-day ENSO is a good analogue for the past.

6 Conclusions

We have presented two new ENSO reconstructions based on temperature- and precipitation-sensitive proxies respectively. The quality of the reconstructions degrades further back in time as there is less proxy data available, which is particularly detrimental to the temperature reconstruction. We find no evidence that the ENSO-driven changes in precipitation and in temperature are in disagreement over the last millennium. The precipitation ENSO reconstruction suggests that the LIA was characterised by a more El Niño-like state compared with the MCA, while there is no discernible difference visible in the temperature reconstruction (Fig. 4). The precipitation results hold when using 20CRv2 as well as GPCP for deriving the precipitation EOF, which is encouraging. The leave-one-out results hint at various possible sources of uncertainty and error, including proxy record length and type. However, excluding suspect proxies did not significantly change the results.

Title Page

Abstract

Introduction

Conclusions

References

Tables

Figures



Back

Close

Full Screen / Esc

Printer-friendly Version

Interactive Discussion



**ENSO
reconstructions**

L. M. K. Henke et al.

[Title Page](#)[Abstract](#)[Introduction](#)[Conclusions](#)[References](#)[Tables](#)[Figures](#)[Back](#)[Close](#)[Full Screen / Esc](#)[Printer-friendly Version](#)[Interactive Discussion](#)

A major limitation on our ability to accurately reconstruct ENSO back in time is the lack of high-quality, long proxy records in the tropical and subtropical latitude bands and we reiterate the need for continued efforts to collect such data. The pseudoproxy experiments described in this paper can quite easily be adapted to search for optimal locations from which additional proxy information would be the most beneficial, as previously done specifically for corals by Evans et al. (1998) (see also Comboul et al., 2015, for a recent endeavour). A final caveat is the reliance on modern-day ENSO patterns and the implicit assumption of its stationarity through time. Hopefully continued improvements in the ability of GCMs to accurately simulate and reproduce ENSO behaviour in conjunction with more high-quality proxy data will give both the palaeocommunity and the modelling community an increasingly reliable foundation for creating, calibrating and evaluating palaeo-ENSO reconstructions.

Appendix A: Proxy data details

Tables 1 and 2 provide an overview of the proxy records collected for this study. Where a proxy was rejected, the reason is given. “AOI” refers to a proxy not being selected for any networks by the “add-one-in” algorithm. This could be due to poor ability to capture the EOF pattern related to location or time resolution. Records from the NOAA Paleoclimate Database are identified by original publications. Where there are multiple timeseries from one record, an identifier suffix is added. The naming of this identifier is always based on the naming in the original database files.

Most tree ring records were taken from the dataset used by Mann et al. (2008), which is a reduced set derived from the International Tree Ring Data Bank (ITRDB, version 5.03; www.ncdc.noaa.gov/paleo/treering.html). The naming for these series has not changed from the original (an abbreviated location followed by a core number). The tree ring series were subject to the following selection criteria (Mann et al., 2008):

- (i) series must cover at least the interval 1750 to 1970, (ii) correlation between individual cores for a given site must be 0.50 for this period, (iii)

ENSO reconstructions

L. M. K. Henke et al.

Title Page

Abstract

Introduction

Conclusions

References

Tables

Figures



Back

Close

Full Screen / Esc

Printer-friendly Version

Interactive Discussion



there must be at least eight samples during the screened period 1800–1960 and for every year used. Series that were redundant with other compilations [used in the Mann et al. (2008) study] were not included. Four other series were not included because of site-specific problems [...]. Of the remaining series, [some] had to be replaced because of format errors in the chronology file on the ITRDB [...], or because sample depth data were missing from the chronology file. [...] When sample depth data were absent, the raw ring-width data from ITRDB were used to recalculate the chronology using program ARSTAN (Version 6.05P), with the following settings: (a) a single detrending fitting a cubic spline of 50% variance reduction function at 66.6% the length of each sample, no stabilization of variance or autoregressive modeling, indices computed as ratio, that is measurement divided by curve, and chronology calculated as biweight robust mean estimate.

Additional tree ring records were retrieved from the NOAA Paleoclimatology Database (<http://www.ncdc.noaa.gov/data-access/paleoclimatology-data/datasets>) and were used as presented there. Where available, temperature or precipitation converted series were used. This was done to minimise biases due to nonlinearities in the raw proxy data which are accounted for in the conversion process. In some cases, two precipitation series were available for different seasons; these were summed to get a better approximate of an annual signal. While this may not be entirely accurate, annual signals are more desirable for the purpose of this study. Moreover, summing the records as opposed to treating them as individual records makes very little difference due to the nature of the method (weighting and summing the series). For coral records, spliced records were used where possible to maximise the length.

Appendix B: Detailed methods

The method developed in this study was used to create separate temperature and precipitation-based ENSO reconstructions made from weighted temperature and pre-

5 precipitation proxy records respectively. The weights were based on Empirical Orthogonal Function (EOF) patterns derived from the Twentieth Century Reanalysis Project Version 2 (20CRv2). The EOFs were selected on the basis of their ability to represent the precipitation and temperature signatures of ENSO. The available proxy records were
10 combined into 1000 “optimal” proxy networks using a pseudoproxy approach to automatically select the best combinations in the presence of white noise. This also acted to filter out proxies whose resolution, length or timespan were unfavourable. Each network was then used to create an ENSO timeseries with an associated error range. The final ENSO reconstruction was taken as the mean of all network timeseries, with an
15 uncertainty envelope determined by the ensemble range and the 5–95th percentile of individual members’ error ranges. Each step is described in more detail below.

B1 Pre-processing the data

All proxy timeseries were first averaged or interpolated to 30 year values. Since the proxy data have different units and cannot be compared directly, they were all normalised to a common period ($a : b$) where all proxies contain data within the network
20 via the equation:

$$\text{Pnorm}_t = \frac{P_t - \mu_{a:b}}{\sigma_{a:b}} \quad (\text{B1})$$

where Pnorm_t is the normalised proxy value at time t , P_t is the original value at time t , $\mu_{a:b}$ is the mean value of proxy P between common period $a : b$, and $\sigma_{a:b}$ is the corresponding standard deviation. The length of $a : b$ was ensured to be at least 100 years to reduce the probability of μ and σ being dominated by noise. In some cases this led to rejection of some proxies due to their length or their starting or ending too late or too early compared to the other records. This process of normalisation is similar to the method used in Wilson et al. (2010). To reduce overrepresentation of more densely
25 sampled locations, proxies that fell in the same grid box were averaged after normalisation.

ENSO reconstructions

L. M. K. Henke et al.

Title Page

Abstract

Introduction

Conclusions

References

Tables

Figures



Back

Close

Full Screen / Esc

Printer-friendly Version

Interactive Discussion



B2 Method calibration and validation

When performing pseudoproxy experiments, it is important to implement some form of verification of the results. Cross-validation is frequently used for testing the quality of statistical reconstruction and prediction methods (Mann et al., 2007; Emile-Geay et al., 2013a; Stahle et al., 1998). It involves testing the method using independent data; that is, data that is not used to develop the method. Here, this is done by separating the 20CRv2 data into a “training” (1950–2010) and a “validation” (1871–1949) set. This division is based on the fact that a higher percentage of the more recent reanalysis data is computed from observational data rather than model infilling. It is thus of higher quality and more likely to give a realistic EOF pattern to use for calibrating the proxy networks. It could also be argued that the validation testing is more stringent, as the validation data is more likely to contain noise or inaccuracies and thus lower the validation scores.

There are several measures of quality for validation statistics, the most common of which are the coefficient of determination R^2 , the reduction of error (RE) and the coefficient of efficiency (CE). Comprehensive discussions on the relative merits and pitfalls of these measures can be found in the literature (cf. Cook et al., 1995; Emile-Geay et al., 2013a). We chose to use CE as it is more stringent than RE and is more suitable for low-frequency reconstruction skill than R^2 (Bürger, 2007; Emile-Geay et al., 2013a). CE is calculated as follows:

$$CE = 1 - \frac{\sum_{i=1}^n (z - \hat{z})^2}{\sum_{i=1}^n (z - \mu_v)^2} \quad (\text{B2})$$

Where z is the observed value, \hat{z} is the estimated value, and μ_v is the mean of z over the validation period. CE scores range from $-\infty$ to $+1$, with 1 being a perfect score. The remaining methods sections further elaborate on where the training and validation partitioning comes into effect.

CPD

11, 5549–5604, 2015

ENSO
reconstructions

L. M. K. Henke et al.

Title Page

Abstract

Introduction

Conclusions

References

Tables

Figures

◀

▶

◀

▶

Back

Close

Full Screen / Esc

Printer-friendly Version

Interactive Discussion



B3 EOF calculation

Empirical Orthogonal Function (EOF) analysis decomposes a spatiotemporal dataset into stationary time-varying coefficients. For a dataset of spatial resolution $x \times y$ and n time steps, it produces n maps (EOFs) of $x \times y$. The first map (EOF1) captures the largest fraction of variance of the original data. Each subsequent map maximises the amount of remaining variance captured, while being completely uncorrelated (orthogonal) to all preceding maps. Every EOF map is accompanied by a principal component (PC) timeseries of length n , which describes how the magnitude and sign of the EOF pattern varies throughout the dataset. The first few EOFs can usually be attributed to physical dynamical phenomena such as seasonality or ENSO. By only retaining the leading EOFs, a dataset can be “cleaned” of the (assumedly) random noise captured by the lower-order EOFs.

EOF analysis was applied to the training set of the normalised 20CRv2 annual mean surface temperature and precipitation rate datasets to extract ENSO-like temperature and precipitation patterns respectively. The data were not detrended prior to EOF calculation as this may remove some information about long-term trends in ENSO variability. The time series correlation of the normalised vs. non-normalised ENSO EOFs was very high ($R^2 > 0.74$ for 20CRv2 and GPCP, not shown). In both temperature and precipitation, the first EOF displayed the signature ENSO pattern and was thus selected as a basis for weighting the proxies. PCs were calculated for the full (PC_{t+v}), training (PC_t) and validation (PC_v) datasets.

B4 Optimal proxy network creation

After screening proxy records as described in Sect. 2.1, a pseudoproxy experiment was conducted to create an “optimal network” ensemble. Since there is no straightforward way of assessing the quality or relevance of a proxy beyond the selection criteria already discussed, a pseudoproxy approach can aid in making a more objective and refined decision on how to optimise the use of available proxy data (Smerdon, 2012).

CPD

11, 5549–5604, 2015

ENSO
reconstructions

L. M. K. Henke et al.

Title Page

Abstract

Introduction

Conclusions

References

Tables

Figures



Back

Close

Full Screen / Esc

Printer-friendly Version

Interactive Discussion



ENSO reconstructions

L. M. K. Henke et al.

Title Page

Abstract

Introduction

Conclusions

References

Tables

Figures



Back

Close

Full Screen / Esc

Printer-friendly Version

Interactive Discussion



Since for pseudoproxies the “ideal world” is known (in this case the 20CRv2 derived EOFs and PCs), it is possible to quantify the skill of the reconstruction. While a “blanket” approach (in which every available record is used) may sound attractive, it increases the risk that some covarying, non-white noise in a subset of the proxies skews the resulting reconstruction. This is, for example, pertinent in North America where there is high clustering of tree ring records. Testing showed that when all records were added to the reconstruction, a regional non-ENSO trend obscured the ENSO signal (not shown). The only case in which it is certain that using all available proxies is preferred, is when each gridbox contains a non-climatic noise-free proxy such that the network gives complete spatial and temporal coverage.

For the pseudoproxy experiment, the 20CRv2 datasets were first replicated in the time dimension to get a length of 1000 years. Pseudoproxies were created by taking timeseries from the reanalysis datasets at real proxy locations and applying the real proxies’ temporal resolution between 100–1100 yr BP; this period was chosen as it is the focus of this study. The resolution was recreated by assuming that each data point represents an average of the previous unsampled years; for example in a proxy with a 10 year resolution, data point n was recreated by taking the average over points $(n - 9) : n$. White Gaussian noise was added with a signal-to-noise ratio (SNR) of 0.4, which is considered a realistic average ratio for climate proxies (Mann et al., 2007; Smerdon, 2012). Data on real SNRs is sparse in the original literature. Lastly, the pseudoproxies were averaged to 30 years, as our focus is on long-term ENSO state rather than inter-annual variability.

The “optimal” network algorithm is an “add-one-in” methodology whereby pseudoproxies derived from the $(t + v)$ 20CRv2 dataset were added one by one to find the combination that produced the highest correlation with the expected outcome (i.e. the PC_{t+v} timeseries). The use of the full $t + v$ was necessary to enable the calculation of 30 year means. While this somewhat compromises the independence of the validation, using only the calibration dataset of 50 years would likely have been more detrimental.

The important separation here is between the EOF pattern (derived from the training data) and the calculation of the validation statistic CE (using μ_v).

The ENSO reconstruction procedure described below in 3.1 was run repeatedly, starting with a “base” network of zero proxies and adding each proxy separately. Once all networks had been tested individually, the proxy whose reconstruction (ENSO) gave the best CE value (using $z = PC_{t+v}$, $\hat{z} = ENSO$ and $\mu_v = PC_v$) was added to the base network. This process was repeated with the remaining proxies until all proxies were incorporated in the base network. The proxy combination which gave the overall highest CE was then saved as the “optimal” network. Finally, the entire process from creating pseudoproxies to selecting the optimal network was repeated 1000 times using different noise in each run.

The add-one-in method picks proxy combinations based on an improvement in CE, but it does not necessarily guarantee that the final network actually produces a good ENSO reconstruction. This was tested by comparing the pseudoproxy CE to a threshold value CE_{crit} . This critical value was calculated for each network by running 1000 ENSO reconstructions replacing the (signal+noise) pseudoproxy series in the network with pure noise, and calculating the 95th percentile of their CE values. To compare, 1000 pseudoproxy ENSOs were also made; if 95% of the pseudoproxy CE values were higher than CE_{crit} , the network was deemed to be useful and was retained for the final reconstruction.

The combination of using pseudoproxies, the add-one-in approach and CE_{crit} simultaneously accounts for proxy temporal resolution, spatial distribution and temporal coverage (i.e. proxy start and end dates), and gives an estimate of the uncertainty due to proxy noise. However, an important assumption is that the signal in all proxies is solely temperature or precipitation, and it is thus still a “best case” estimate.

B5 EOF-weighted ENSO reconstruction

The “optimal” networks that passed the CE test were used to create an ensemble of real proxy ENSO reconstructions. The remaining ones may not all be unique, further reduc-

ENSO reconstructions

L. M. K. Henke et al.

Title Page

Abstract

Introduction

Conclusions

References

Tables

Figures



Back

Close

Full Screen / Esc

Printer-friendly Version

Interactive Discussion



ing the effective number of networks. Multiply occurring networks are assumedly more effective proxy combinations; retaining the duplicates accordingly upweights these networks in the final reconstruction. The ENSO reconstruction for each ensemble member (network) was conducted in a series of steps: calculating proxy weights, combining the proxy records into ENSO reconstructions, calculating mean squared errors, and creating a proxy reconstruction ensemble. Each step is explained in more detail below.

B5.1 Proxy weighting and ENSO reconstruction

The proxy weights were determined by the EOF pattern derived from 20CRv2. The value of this EOF indicates to what extent the precipitation or temperature is expected to be influenced by ENSO at a given location, with highly negative and highly positive regions displaying strong ENSO linkages. Each normalised proxy P at location $[x, y]$ was multiplied by a scaled version of the EOF value at location $[x, y]$. The scaling was such that at each timestep the absolute sum of the weights was 1, which accounts for the fact that the number of locations with proxy data varies over the reconstructed period (especially the beginning and end). The weight of a given proxy location i can thus be considered an indication of the location's relative sensitivity to ENSO which changes depending on the number of proxies n available at each timestep and their associated EOF values:

$$\text{EOFnorm}_i = \frac{\text{EOF}_i}{\sum_{i=1}^n |\text{EOF}_i|} \quad (\text{B3})$$

Once weighted, the proxy records were summed to obtain a single timeseries to make an ENSO reconstruction.

B5.2 Error estimation

Error estimates for the ENSO reconstructions were derived again using a pseudoproxy method similar to the optimal networks creation. As the proxy availability varies over

ENSO reconstructions

L. M. K. Henke et al.

Title Page

Abstract

Introduction

Conclusions

References

Tables

Figures



Back

Close

Full Screen / Esc

Printer-friendly Version

Interactive Discussion



**ENSO
reconstructions**

L. M. K. Henke et al.

[Title Page](#)[Abstract](#)[Introduction](#)[Conclusions](#)[References](#)[Tables](#)[Figures](#)[Back](#)[Close](#)[Full Screen / Esc](#)[Printer-friendly Version](#)[Interactive Discussion](#)

time, root mean square errors (RMSEs) were calculated for each timestep separately. This was done by calculating the RMSE for a network that only contains the proxies available at that timestep: for reconstruction ensemble network n , the proxies available at time t were used as a “frozen” (unchanging) network to create 1000 pseudo-reconstructions from which RMSE values were calculated for time t . Repeated for each timestep, this resulted in 1000 absolute error value timeseries for each network n . This was translated into ensemble member uncertainty limits by adding and subtracting the 1000 error series from the ENSO timeseries (to get the maximum and minimum error limits respectively) and taking the 5–95th percentile over their full range. This error estimation explicitly takes into account the impact of network choice as well as random error affecting the proxies.

B5.3 Proxy ENSO ensemble

Once ENSO reconstructions and associated uncertainty estimates were calculated for all networks (ensemble members), they were renormalised to 100–650 yr BP to make the trends and amplitudes comparable, within and between temperature and precipitation. The period 100–650 yr BP was chosen because it was common to all ENSO timeseries and only covers one of the two periods of interest (the LIA). Although calibration to the instrumental period would potentially allow us to quantify the ENSO amplitudes, this was not done for two reasons. Firstly, the proxy data coverage during the instrumental period and the preceding century was relatively low, reducing the confidence in the reconstruction during that period; calibrating to this period would thus increase the uncertainty on the rest of the reconstruction. Secondly, any calibration to the instrumental data is necessarily biased towards high-frequency trends (Mann et al., 2008). Within a 30 year averaged series, the number of comparison points with the instrumental period is extremely low. The final proxy ENSO reconstruction was calculated as the ensemble mean. The corresponding error estimate is a combination of the reconstruction ensemble range and the error ranges for individual ensemble members.

Acknowledgements. Many thanks to the Databases of the NOAA World Data Center for Paleoclimatology and Pangaea and all contributing authors for making available the proxy data used in this study.

The GPCP and 20th Century Reanalysis V2 data were provided by the NOAA/OAR/ESRL PSD, Boulder, Colorado, USA, from their Web site at <http://www.esrl.noaa.gov/psd/>.

Support for the Twentieth Century Reanalysis Project dataset is provided by the US Department of Energy, Office of Science Innovative and Novel Computational Impact on Theory and Experiment (DOE INCITE) program, and Office of Biological and Environmental Research (BER), and by the National Oceanic and Atmospheric Administration Climate Program Office.

The GPCP combined precipitation data were developed and computed by the NASA/Goddard Space Flight Center's Laboratory for Atmospheres as a contribution to the GEWEX Global Precipitation Climatology Project.

L. Henke was supported by a University of Exeter Climate Change and Sustainable Futures studentship.

References

Abram, N. J., McGregor, H. V., Gagan, M. K., Hantoro, W. S., and Suwargadi, B. W.: Oscillations in the southern extent of the Indo-Pacific Warm Pool during the mid-Holocene, *Quaternary Sci. Rev.*, 28, 2794–2803, doi:10.1016/j.quascirev.2009.07.006, 2009. 5594

Anchukaitis, K. J. and Evans, M. N.: Tropical cloud forest climate variability and the demise of the Monteverde golden toad, *P. Natl. Acad. Sci. USA*, 107, 5036–5040, doi:10.1073/pnas.0908572107, 2010. 5593

Anderson, L.: Holocene record of precipitation seasonality from lake calcite $\delta^{18}\text{O}$ in the central Rocky Mountains, United States, *Geology*, 39, 211–214, doi:10.1130/G31575.1, 2011. 5593

Asmerom, Y., Polyak, V., Burns, S. J., and Rasmussen, J.: Solar forcing of Holocene climate: new insights from a speleothem record, southwestern United States, *Geology*, 35, 1–4, doi:10.1130/G22865A.1, 2007. 5593

Badjeck, M.-C., Allison, E. H., Halls, A. S., and Dulvy, N. K.: Impacts of climate variability and change on fishery-based livelihoods, *Mar. Policy*, 34, 375–383, doi:10.1016/j.marpol.2009.08.007, 2010. 5551

Title Page

Abstract

Introduction

Conclusions

References

Tables

Figures



Back

Close

Full Screen / Esc

Printer-friendly Version

Interactive Discussion



ENSO reconstructions

L. M. K. Henke et al.

Title Page

Abstract

Introduction

Conclusions

References

Tables

Figures



Back

Close

Full Screen / Esc

Printer-friendly Version

Interactive Discussion



- Bale, R. J., Robertson, I., Salzer, M. W., Loader, N. J., Leavitt, S. W., Gagen, M., Harlan, T. P., and McCarroll, D.: An annually resolved bristlecone pine carbon isotope chronology for the last millennium, *Quaternary Res.*, 76, 22–29, doi:10.1016/j.yqres.2011.05.004, 2011. 5593
- 5 Barron, J. A.: High-resolution climatic evolution of coastal northern California during the past 16 000 years, *Paleoceanography*, 18, 1020, doi:10.1029/2002PA000768, 2003. 5594
- Barron, J. A. and Anderson, L.: Enhanced Late Holocene ENSO/PDO expression along the margins of the eastern North Pacific, *Quatern. Int.*, 235, 3–12, doi:10.1016/j.quaint.2010.02.026, 2011. 5552
- 10 Bellenger, H., Guilyardi, E., Leloup, J., Lengaigne, M., and Vialard, J.: ENSO representation in climate models: From CMIP3 to CMIP5, *Clim. Dynam.*, 42, 1999–2018, doi:10.1007/s00382-013-1783-z, 2014. 5551
- Bird, B. W., Abbott, M. B., Rodbell, D. T., and Vuille, M.: Holocene tropical South American hydroclimate revealed from a decadal resolved lake sediment $\delta^{18}\text{O}$ record, *Earth Planet. Sc. Lett.*, 310, 192–202, doi:10.1016/j.epsl.2011.08.040, 2011. 5593
- 15 Boiseau, M., Ghil, M., and Juillet-leclerc, A.: Climatic trends and interdecadal variability from South-Central Pacific coral records, *Geophys. Res. Lett.*, 26, 2881–2884, 1999. 5594
- Bonnefille, R. and Chalie, F.: Pollen-inferred precipitation time-series from equatorial mountains, Africa, the last 40 kyr BP, *Global Planet. Change*, 26, 25–50, doi:10.1016/S0921-8181(00)00032-1, 2000. 5593
- 20 Braganza, K., Gergis, J. L., Power, S. B., Risbey, J. S., and Fowler, A. M.: A multiproxy index of the El Niño-Southern Oscillation, A.D. 1525–1982, *J. Geophys. Res.-Atmos.*, 114, 1–17, doi:10.1029/2008JD010896, 2009. 5554, 5566
- Brook, G., Sheen, S.-W., Rafter, M., Railsback, L. B., and Lundberg, J.: A high-resolution proxy record of rainfall and ENSO since AD 1550 from layering in stalagmites from Anjohibe Cave, Madagascar, Holocene, 9, 695–705, doi:10.1191/095968399677907790, 1999. 5552
- 25 Buckley, B. M., Anchukaitis, K. J., Penny, D., Fletcher, R., Cook, E. R., Sano, M., Nam, L. C., Wichienkeo, A., Minh, T. T., and Hong, T. M.: Climate as a contributing factor in the demise of Angkor, Cambodia, *P. Natl. Acad. Sci. USA*, 107, 6748–6752, doi:10.1073/pnas.0910827107, 2010. 5593
- 30 Buizer, J. L., Foster, J., and Lund, D.: Global impacts and regional actions: Preparing for the 1997-98 El Niño, *B. Am. Meteorol. Soc.*, 81, 2121–2139, doi:10.1175/1520-0477(2000)081<2121:GIARAP>2.3.CO;2, 2000. 5551

ENSO reconstructions

L. M. K. Henke et al.

Title Page

Abstract

Introduction

Conclusions

References

Tables

Figures



Back

Close

Full Screen / Esc

Printer-friendly Version

Interactive Discussion



- Bürger, G.: On the verification of climate reconstructions, *Clim. Past Discuss.*, 3, 249–284, doi:10.5194/cpd-3-249-2007, 2007. 5573
- Cane, M. A.: The evolution of El Niño, past and future, *Earth Planet. Sc. Lett.*, 230, 227–240, doi:10.1016/j.epsl.2004.12.003, 2005. 5552
- 5 Carré, M., Bentaleb, I., Fontugne, M., and Lavallée, D.: Strong El Niño events during the early Holocene: stable isotope evidence from Peruvian sea shells, *Holocene*, 15, 42–47, doi:10.1191/0959683605h1782rp, 2005. 5552
- Christie, D. A., Boninsegna, J. A., Cleaveland, M. K., Lara, A., Le Quesne, C., Morales, M. S., Mudelsee, M., Stahle, D. W., and Villalba, R.: Aridity changes in the Temperate-Mediterranean transition of the Andes since AD 1346 reconstructed from tree-rings, *Clim. Dynam.*, 36, 1505–1521, doi:10.1007/s00382-009-0723-4, 2011. 5593
- 10 Cleaveland, M. K., Stahle, D. W., Therrell, M. D., Villanueva-Diaz, J., and Burns, B. T.: Tree-ring reconstructed winter precipitation and tropical teleconnections in Durango, Mexico, *Climate Change*, 59, 369–388, doi:10.1023/A:1024835630188, 2003. 5593
- 15 Clement, A. C., Cane, M. A., and Seager, R.: An orbitally driven tropical source for abrupt climate change, *J. Climate*, 14, 2369–2375, doi:10.1175/1520-0442(2001)014<2369:AODTSF>2.0.CO;2, 2001. 5552
- Coats, S., Smerdon, J. E., Cook, B. I., and Seager, R.: Stationarity of the tropical pacific teleconnection to North America in CMIP5/PMIP3 model simulations, *Geophys. Res. Lett.*, 40, 4927–4932, doi:10.1002/grl.50938, 2013. 5564
- 20 Cobb, K. M., Charles, C. D., Cheng, H., and Edwards, R. L.: El Niño/Southern Oscillation and tropical Pacific climate during the last millennium, *Nature*, 424, 271–276, doi:10.1038/nature01779, 2003. 5595
- Cole, J. E., Fairbanks, R. G., and Shen, G. T.: Recent variability in the southern oscillation: isotopic results from a Tarawa Atoll coral, *Science*, 260, 1790–1793, doi:10.1126/science.260.5115.1790, 1993. 5593
- 25 Collins, M.: El Nino- or La Nina-like climate change?, *Clim. Dynam.*, 24, 89–104, doi:10.1007/s00382-004-0478-x, 2005. 5551
- Comboul, M., Emile-Geay, J., Evans, M. N., Mirnateghi, N., Cobb, K. M., and Thompson, D. M.: A probabilistic model of chronological errors in layer-counted climate proxies: applications to annually banded coral archives, *Clim. Past*, 10, 825–841, doi:10.5194/cp-10-825-2014, 2014. 5568
- 30

[Title Page](#)[Abstract](#)[Introduction](#)[Conclusions](#)[References](#)[Tables](#)[Figures](#)[Back](#)[Close](#)[Full Screen / Esc](#)[Printer-friendly Version](#)[Interactive Discussion](#)

- Comboul, M., Emile-geay, J., Hakim, G. J., and Evans, M. N.: Paleoclimate sampling as a sensor placement problem, *J. Climate*, 28, 7717–7740, 2015. 5570
- Compo, G. P., Whitaker, J. S., Sardeshmukh, P. D., Matsui, N., Allan, R. J., Yin, X., Gleason, B. E., Vose, R. S., Rutledge, G., Bessemoulin, P., Bronnimann, S., Brunet, M., Crouthamel, R. I., Grant, A. N., Groisman, P. Y., Jones, P. D., Kruk, M. C., Kruger, A. C., Marshall, G. J., Maugeri, M., Mok, H. Y., Nordli, O., Ross, T. F., Trigo, R. M., Wang, X. L., Woodruff, S. D., and Worley, S. J.: The Twentieth Century Reanalysis Project, *Q. J. Roy. Meteor. Soc.*, 137, 1–28, doi:10.1002/qj.776, 2011. 5555
- Conroy, J., Overpeck, J. T., and Cole, J. E.: El Niño-Southern Oscillation and changes in the zonal gradient of tropical Pacific sea surface temperature over the last 1.2 ka, *PAGES News*, 18, 1–5, 2010. 5565
- Conroy, J. L., Overpeck, J. T., Cole, J. E., Shanahan, T. M., and Steinitz-Kannan, M.: Holocene changes in eastern tropical Pacific climate inferred from a Galápagos lake sediment record, *Quaternary Sci. Rev.*, 27, 1166–1180, doi:10.1016/j.quascirev.2008.02.015, 2008. 5565, 5566, 5568, 5593
- Conroy, J. L., Restrepo, A., Overpeck, J. T., Steinitz-Kannan, M., Cole, J. E., Bush, M. B., and Colinvaux, P. A.: Unprecedented recent warming of surface temperatures in the eastern tropical Pacific Ocean, *Nat. Geosci.*, 2, 46–50, doi:10.1038/ngeo390, 2009. 5593
- Cook, E. R., Briffa, K. R., Meko, D. M., Graybill, D. A., and Funkhouser, G.: The “segment length curse” in long tree-ring chronology development for palaeoclimatic studies, *Holocene*, 5, 229–237, 1995. 5554, 5555, 5563, 5573
- Cook, E. R., Buckley, B. M., D’Arrigo, R. D., and Peterson, M. J.: Warm-season temperatures since 1600 BC reconstructed from Tasmanian tree rings and their relationship to large-scale sea surface temperature anomalies, *Clim. Dynam.*, 16, 79–91, doi:10.1007/s003820050006, 2000. 5595
- Crausbay, S. D., Russell, J. M., and Schnurrenberger, D. W.: A ca. 800-year lithologic record of drought from sub-annually laminated lake sediment, East Java, *J. Paleolimnol.*, 35, 641–659, doi:10.1007/s10933-005-4440-7, 2006. 5552
- Cronin, T. M., Dwyer, G. S., Kamiya, T., Schwede, S., and Willard, D. A.: Medieval Warm Period, Little Ice Age and 20th century temperature variability from Chesapeake Bay, *Global Planet. Change*, 36, 17–29, doi:10.1016/S0921-8181(02)00161-3, 2003. 5595
- Damassa, T. D., Cole, J. E., Barnett, H. R., Ault, T. R., and McClanahan, T. R.: Enhanced multidecadal climate variability in the seventeenth century from coral isotope records in the

western Indian Ocean, *Paleoceanography*, 21, PA2016, doi:10.1029/2005PA001217, 2006. 5595

DeLong, K. L., Quinn, T. M., Taylor, F. W., Lin, K., and Shen, C.-C.: Sea surface temperature variability in the southwest tropical Pacific since AD 1649, *Nature Climate Change*, 2, 799–804, doi:10.1038/nclimate1583, 2012. 5595

Díaz, S. C., Therrell, M. D., Stahle, D. W., and Cleaveland, M. K.: Chihuahua (Mexico) winter-spring precipitation reconstructed from tree-rings, 1647–1992, *Clim. Res.*, 22, 237–244, doi:10.3354/cr022237, 2002. 5593

Emile-Geay, J., Cobb, K. M., Mann, M. E., and Wittenberg, A. T.: Estimating central equatorial Pacific SST variability over the past millennium. Part I: Methodology and validation, *J. Climate*, 26, 2302–2328, doi:10.1175/JCLI-D-11-00510.1, 2013a. 5567, 5573

Emile-Geay, J., Cobb, K. M., Mann, M. E., and Wittenberg, A. T.: Estimating central equatorial Pacific SST variability over the past millennium. Part II: Reconstructions and Implications, *J. Climate*, 26, 2329–2352, doi:10.1175/JCLI-D-11-00511.1, 2013b. 5566, 5568

Esper, J., Cook, E. R., and Schweingruber, F. H.: Low-frequency signals in long tree-ring chronologies for reconstructing past temperature variability, *Science*, 295, 2250–2253, doi:10.1126/science.1066208, 2002. 5555

Evans, M. N., Kaplan, A., and Cane, M. A.: Optimal sites for coral-based reconstruction of global sea surface temperature, *Paleoceanography*, 13, 502–516, doi:10.1029/98PA02132, 1998. 5570

Evans, M. N., Tolwinski-Ward, S. E., Thompson, D. M., and Anchukaitis, K. J.: Applications of proxy system modeling in high resolution paleoclimatology, *Quaternary Sci. Rev.*, 76, 16–28, 2013. 5568

Faulstich, H. L., Woodhouse, C. A., and Griffin, D.: Reconstructed cool- and warm-season precipitation over the tribal lands of northeastern Arizona, *Climate Change*, 118, 457–468, doi:10.1007/s10584-012-0626-y, 2013. 5593

Felis, T., Suzuki, A., Kuhnert, H., Rambu, N., and Kawahata, H.: Pacific decadal oscillation documented in a coral record of North Pacific winter temperature since 1873, *Geophys. Res. Lett.*, 37, 2000–2005, doi:10.1029/2010GL043572, 2010. 5595

Gallant, A. J. E., Phipps, S. J., Karoly, D. J., Mullan, A. B., and Lorrey, A. M.: Nonstationary Australasian teleconnections and implications for paleoclimate reconstructions, *J. Climate*, 26, 8827–8849, doi:10.1175/JCLI-D-12-00338.1, 2013. 5564

CPD

11, 5549–5604, 2015

ENSO reconstructions

L. M. K. Henke et al.

Title Page

Abstract

Introduction

Conclusions

References

Tables

Figures



Back

Close

Full Screen / Esc

Printer-friendly Version

Interactive Discussion



ENSO reconstructions

L. M. K. Henke et al.

Title Page

Abstract

Introduction

Conclusions

References

Tables

Figures



Back

Close

Full Screen / Esc

Printer-friendly Version

Interactive Discussion



Gergis, J. L. and Fowler, A. M.: How unusual was late 20th century El Niño-Southern Oscillation (ENSO)? Assessing evidence from tree-ring, coral, ice-core and documentary palaeoarchives, A.D. 1525–2002, *Adv. Geosci.*, 6, 173–179, doi:10.5194/adgeo-6-173-2006, 2006. 5566

5 Gergis, J. L. and Fowler, A. M.: A history of ENSO events since AD 1525: implications for future climate change, *Climat Change*, 92, 343–387, doi:10.1007/s10584-008-9476-z, 2009. 5566

Gomez, B., Carter, L., Trustrum, N. A., Palmer, A. S., and Roberts, A. P.: El Niño-Southern Oscillation signal associated with middle Holocene climate change in intercorrelated terrestrial and marine sediment cores, North Island, New Zealand, *Geology*, 32, 653–656, doi:10.1130/G20720.1, 2004. 5552

10 Graham, N. E., Hughes, M. K., Ammann, C. M., Cobb, K. M., Hoerling, M. P., Kennett, D. J., Kennett, J. P., Rein, B., Stott, L., Wigand, P. E., and Xu, T.: Tropical Pacific – mid-latitude teleconnections in medieval times, *Climat Change*, 83, 241–285, doi:10.1007/s10584-007-9239-2, 2007. 5566

15 Griffin, D., Woodhouse, C. A., Meko, D. M., Stahle, D. W., Faulstich, H. L., Carrillo, C., Touchan, R., Castro, C. L., and Leavitt, S. W.: North American monsoon precipitation reconstructed from tree-ring latewood, *Geophys. Res. Lett.*, 40, 954–958, doi:10.1002/grl.50184, 2013. 5593

20 Guilyardi, E., Wittenberg, A., Fedorov, A., Collins, M., Wang, C., Capotondi, A., van Oldenborgh, G. J., and Stockdale, T.: Understanding El Niño in ocean-atmosphere general circulation models: Progress and challenges, *B. Am. Meteorol. Soc.*, 90, 325–340, doi:10.1175/2008BAMS2387.1, 2009. 5551

Haug, G. H., Hughen, K. A., Sigman, D. M., Peterson, L. C., and Röhl, U.: Southward migration of the intertropical convergence zone through the Holocene, *Science*, 293, 1304–1308, doi:10.1126/science.1059725, 2001. 5552, 5593

25 Hendy, E. J., Gagan, M. K., and Lough, J. M.: Chronological control of coral records using luminescent lines and evidence for non-stationary ENSO teleconnections in northeast Australia, *Holocene*, 13, 187–199, doi:10.1191/0959683603hl606rp, 2003. 5593

30 Hengstum, P. J. V., Donnelly, J. P., Kingston, A. W., Williams, B. E., Scott, D. B., Reinhardt, E. G., Little, S. N., and Patterson, W. P.: Low-frequency storminess signal at Bermuda linked to cooling events in the North Atlantic region, *Paleoceanography*, 30, 52–76, doi:10.1002/2014PA002662, 2015. 5598

ENSO reconstructions

L. M. K. Henke et al.

Title Page

Abstract

Introduction

Conclusions

References

Tables

Figures



Back

Close

Full Screen / Esc

Printer-friendly Version

Interactive Discussion



Hjelle, B. and Glass, G. E.: Outbreak of hantavirus infection in the Four Corners region of the United States in the wake of the 1997–1998 El Niño–Southern Oscillation, *J. Infect. Dis.*, 181, 1569–1573, doi:10.1086/315467, 2000. 5551

Ivanochko, T. S., Ganeshram, R. S., Brummer, G. J. A., Ganssen, G., Jung, S. J. A., Moreton, S. G., and Kroon, D.: Variations in tropical convection as an amplifier of global climate change at the millennial scale, *Earth Planet. Sc. Lett.*, 235, 302–314, doi:10.1016/j.epsl.2005.04.002, 2005. 5552

Jones, P., Briffa, K., Osborn, T., Lough, J., van Ommen, T., Vinther, B., Luterbacher, J., Wahl, E., Zwiers, F., Mann, M., Schmidt, G., Ammann, C., Buckley, B., Cobb, K., Esper, J., Goosse, H., Graham, N., Jansen, E., Kiefer, T., Kull, C., Küttel, M., Mosley-Thompson, E., Overpeck, J., Riedwyl, N., Schulz, M., Tudhope, A., Villalba, R., Wanner, H., Wolff, E. W., Xoplaki, E., Küttel, M., Mosley-Thompson, E., Overpeck, J., Riedwyl, N., Schulz, M., Tudhope, A., Villalba, R., Wanner, H., Wolff, E. W., and Xoplaki, E.: High-resolution palaeoclimatology of the last millennium: a review of current status and future prospects, *Holocene*, 19, 3–49, doi:10.1177/0959683608098952, 2009. 5553

Jones, P. D. and Mann, M. E.: Climate over past millennia, *Rev. Geophys.*, 42, 1–42, doi:10.1029/2003RG000143, 2004. 5554, 5555

Keigwin, L. D.: The Little Ice Age and medieval warm period in the Sargasso Sea, *Science*, 274, 1504–1508, doi:10.1126/science.274.5292.1504, 1996. 5595

Kellerhals, T., Brütsch, S., Sigl, M., Knüsel, S., Gäggeler, H. W., and Schwikowski, M.: Ammonium concentration in ice cores: a new proxy for regional temperature reconstruction?, *J. Geophys. Res.-Atmos.*, 115, 1–8, doi:10.1029/2009JD012603, 2010. 5595

Kennett, D., Breitenbach, S., Aquino, V., Asmerom, Y., Awe, J., Baldini, J., Bartlein, P., Culleton, B., Ebert, C., Jazwa, C., Macri, M., Marwan, N., Polyak, V., Prufer, K., Riddle, H., Sodemann, H., Winterhalder, B., and Haug, G.: Development and disintegration of Maya political systems in response to climate change, *Science*, 788, 788–791, doi:10.1126/science.1226299, 2012. 5593

Khider, D., Jackson, C. S., and Stott, L. D.: Assessing millennial-scale variability during the Holocene: A perspective from the western tropical Pacific, *Paleoceanography*, 29, 143–159, doi:10.1002/2013PA002534, 2014. 5595

Klein, S. A., Soden, B. J., and Lau, N. C.: Remote sea surface temperature variations during ENSO: evidence for a tropical atmospheric bridge, *J. Climate*, 12, 917–932, doi:10.1175/1520-0442(1999)012<0917:RSSTVD>2.0.CO;2, 1999. 5551

ENSO reconstructions

L. M. K. Henke et al.

Title Page

Abstract

Introduction

Conclusions

References

Tables

Figures



Back

Close

Full Screen / Esc

Printer-friendly Version

Interactive Discussion



- Kovats, R. S., Bouma, M. J., Hajat, S., Worrall, E., and Haines, A.: El Niño and health, *Lancet*, 362, 1481–1489, 2003. 5551
- Langton, S. J., Linsley, B. K., Robinson, R. S., Rosenthal, Y., Oppo, D. W., Eglinton, T. I., Howe, S. S., Djajadihardja, Y. S., and Syamsudin, F.: 3500 yr record of centennial-scale climate variability from the Western Pacific Warm Pool, *Geology*, 36, 795–798, doi:10.1130/G24926A.1, 2008. 5552, 5566
- Lewis, S. C. and LeGrande, A. N.: Stability of ENSO and its tropical Pacific teleconnections over the Last Millennium, *Clim. Past Discuss.*, 11, 1579–1613, doi:10.5194/cpd-11-1579-2015, 2015. 5564
- Li, J., Xie, S.-P., Cook, E. R., Morales, M. S., Christie, D. A., Johnson, N. C., Chen, F., D'Arrigo, R., Fowler, A. M., Gou, X., and Fang, K.: El Niño modulations over the past seven centuries, *Nature Climate Change*, 3, 822–826, doi:10.1038/nclimate1936, 2013. 5566
- Makou, M. C., Eglinton, T. I., Oppo, D. W., and Hughen, K. A.: Postglacial changes in El Niño and La Niña behavior, *Geology*, 38, 43–46, doi:10.1130/G30366.1, 2010. 5566
- Mann, M. E., Cane, M. A., Zebiak, S. E., and Clement, A. C.: Volcanic and solar forcing of the tropical Pacific over the past 1000 years, *J. Climate*, 18, 447–456, doi:10.1175/JCLI-3276.1, 2005. 5551
- Mann, M. E., Rutherford, S., Wahl, E., and Ammann, C.: Robustness of proxy-based climate field reconstruction methods, *J. Geophys. Res.-Atmos.*, 112, 1–18, doi:10.1029/2006JD008272, 2007. 5559, 5573, 5575
- Mann, M. E., Zhang, Z., Hughes, M. K., Bradley, R. S., Miller, S. K., Rutherford, S., and Ni, F.: Proxy-based reconstructions of hemispheric and global surface temperature variations over the past two millennia, *P. Natl. Acad. Sci. USA*, 105, 13252–13257, doi:10.1073/pnas.0805721105, 2008. 5555, 5559, 5561, 5570, 5571, 5578
- Mann, M. E., Zhang, Z., Rutherford, S., Bradley, R. S., Hughes, M. K., Shindell, D., Ammann, C., Faluvegi, G., and Ni, F.: Global signatures and dynamical origins of the Little Ice Age and Medieval Climate Anomaly, *Science*, 326, 1256–1260, doi:10.1126/science.1177303, 2009. 5552, 5560, 5565, 5566
- Marchitto, T. M., Muscheler, R., Ortiz, J. D., Carriquiry, J. D., and van Geen, A.: Dynamical response of the tropical Pacific Ocean to solar forcing during the early Holocene, *Science*, 330, 1378–1381, doi:10.1126/science.1194887, 2010. 5596
- Maupin, C. R., Partin, J. W., Shen, C.-C., Quinn, T. M., Lin, K., Taylor, F. W., Banner, J. L., Thirumalai, K., and Sinclair, D. J.: Persistent decadal-scale rainfall variability in the tropical

ENSO reconstructions

L. M. K. Henke et al.

Title Page

Abstract

Introduction

Conclusions

References

Tables

Figures



Back

Close

Full Screen / Esc

Printer-friendly Version

Interactive Discussion



South Pacific Convergence Zone through the past six centuries, *Clim. Past*, 10, 1319–1332, doi:10.5194/cp-10-1319-2014, 2014. 5593

McGregor, H. V., Gagan, M. K., McCulloch, M. T., Hodge, E., and Mortimer, G.: Mid-Holocene variability in the marine ^{14}C reservoir age for northern coastal Papua New Guinea, *Quat. Geochronol.*, 3, 213–225, doi:10.1016/j.quageo.2007.11.002, 2008. 5552

McGregor, S., Timmermann, A., and Timm, O.: A unified proxy for ENSO and PDO variability since 1650, *Clim. Past*, 6, 1–17, doi:10.5194/cp-6-1-2010, 2010. 5566

Medina-Elizalde, M., Burns, S. J., Lea, D. W., Asmerom, Y., von Gunten, L., Polyak, V., Vuille, M., and Karmalkar, A.: High resolution stalagmite climate record from the Yucatán Peninsula spanning the Maya terminal classic period, *Earth Planet. Sc. Lett.*, 298, 255–262, doi:10.1016/j.epsl.2010.08.016, 2010. 5593

Moy, A. D., Seltzer, G. O., Rodbell, D. T., and Andersons, D. M.: Variability of El Niño/Southern Oscillation activity at millennial timescales during the Holocene epoch, *Nature*, 420, 162–165, doi:10.1038/nature01194, 2002. 5552, 5566, 5593

Nelson, D. B., Abbott, M. B., Steinman, B., Polissar, P. J., Stansell, N. D., Ortiz, J. D., Rosenmeier, M. F., Finney, B. P., and Riedel, J.: Drought variability in the Pacific Northwest from a 6,000-yr lake sediment record, *P. Natl. Acad. Sci. USA*, 108, 3870–3875, doi:10.1073/pnas.1009194108, 2011. 5551, 5552, 5593

Oppo, D. W., Rosenthal, Y., and Linsley, B. K.: 2,000-year-long temperature and hydrology reconstructions from the Indo-Pacific warm pool, *Nature*, 460, 1113–1116, doi:10.1038/nature08233, 2009. 5565, 5593, 5597

Page, S. E., Siegert, F., Rieley, J. O., Boehm, H.-D. V., Jaya, A., and Limin, S.: The amount of carbon released from peat and forest fires in Indonesia during 1997, *Nature*, 420, 61–65, doi:10.1038/nature01131, 2002. 5551

Partin, J. W., Cobb, K. M., Adkins, J. F., Clark, B., and Fernandez, D. P.: Millennial-scale trends in west Pacific warm pool hydrology since the Last Glacial Maximum, *Nature*, 449, 452–455, doi:10.1038/nature08125, 2007. 5552, 5593

Partin, J. W., Quinn, T. M., Shen, C. C., Emile-Geay, J., Taylor, F. W., Maupin, C. R., Lin, K., Jackson, C. S., Banner, J. L., Sinclair, D. J., and Huh, C. A.: Multidecadal rainfall variability in south pacific convergence zone as revealed by stalagmite geochemistry, *Geology*, 41, 1143–1146, doi:10.1130/G34718.1, 2013. 5593

Pohl, K., Therrell, M. D., Blay, G. S., Ayotte, N., Hernandez, J. J. C., Castro, S. D., Oviedo, E. C., Elvir, J. A., Elizondo, M. G., Opland, D., Park, J., Pederson, G., Salazar, S. B., Selem, L. V.,

ENSO reconstructions

L. M. K. Henke et al.

Title Page

Abstract

Introduction

Conclusions

References

Tables

Figures



Back

Close

Full Screen / Esc

Printer-friendly Version

Interactive Discussion



- Villanueva-Díaz, J., and Stahle, D. W.: A cool season precipitation reconstruction for Sotillo, Mexico, *Tree-Ring Res.*, 95, 11–19, 2003. 5593
- Powers, L. A., Johnson, T. C., Werne, J. P., Castañeda, I. S., Hopmans, E. C., Sinninghe Damsté, J. S., and Schouten, S.: Organic geochemical records of environmental variability in Lake Malawi during the last 700 years, Part I: The TEX86 temperature record, *Palaeogeogr. Palaeoclimatol.*, 303, 133–139, doi:10.1016/j.palaeo.2010.09.006, 2011. 5597
- Quinn, T. M., Crowley, T. J., Taylor, F. W., Henin, C., Joannot, P., and Join, Y.: A multicentury stable isotope record from a New Caledonia coral: Interannual and decadal sea surface temperature variability in the southwest Pacific since 1657 AD, *Paleoceanography*, 13, 412–426, doi:10.1029/98PA00401, 1998. 5597
- Raible, C. C., Lehner, F., González-Rouco, J. F., and Fernández-Donado, L.: Changing correlation structures of the Northern Hemisphere atmospheric circulation from 1000 to 2100 AD, *Clim. Past*, 10, 537–550, doi:10.5194/cp-10-537-2014, 2014. 5569
- Rasbury, M. and Aharon, P.: ENSO-controlled rainfall variability records archived in tropical stalagmites from the mid-ocean island of Niue, South Pacific, *Geochim. Geophys. Res.*, 7, Q07010, doi:10.1029/2005GC001232, 2006. 5593
- Reuter, J., Stott, L., Khider, D., Sinha, A., Cheng, H., and Edwards, R. L.: A new perspective on the hydroclimate variability in northern South America during the Little Ice Age, *Geophys. Res. Lett.*, 36, 1–5, doi:10.1029/2009GL041051, 2009. 5593
- Richey, J. N., Poore, R. Z., Flower, B. P., Quinn, T. M., and Hollander, D. J.: Regionally coherent Little Ice Age cooling in the Atlantic Warm Pool, *Geophys. Res. Lett.*, 36, 3–7, doi:10.1029/2009GL040445, 2009. 5597
- Rodbell, D. T.: An 15 000-year record of El Niño-driven alluviation in southwestern Ecuador, *Science*, 283, 516–520, doi:10.1126/science.283.5401.516, 1999. 5593
- Rodysill, J. R., Russell, J. M., Bijaksana, S., Brown, E. T., Safiuddin, L. O., and Eggermont, H.: A paleolimnological record of rainfall and drought from East Java, Indonesia during the last 1400 years, *J. Paleolimnol.*, 47, 125–139, doi:10.1007/s10933-011-9564-3, 2012. 5593
- Russell, J. M. and Johnson, T. C.: Little ice age drought in equatorial Africa: intertropical convergence zone migrations and El Niño-Southern oscillation variability, *Geology*, 35, 21–24, doi:10.1130/G23125A.1, 2007. 5593
- Russon, T., Tudhope, A. W., Hegerl, G. C., Collins, M., and Tindall, J.: Inter-annual tropical Pacific climate variability in an isotope-enabled CGCM: implications for interpreting coral

ENSO reconstructions

L. M. K. Henke et al.

Title Page

Abstract

Introduction

Conclusions

References

Tables

Figures



Back

Close

Full Screen / Esc

Printer-friendly Version

Interactive Discussion



stable oxygen isotope records of ENSO, *Clim. Past*, 9, 1543–1557, doi:10.5194/cp-9-1543-2013, 2013. 5568

Sachs, J. P., Sachse, D., Smittenberg, R. H., Zhang, Z., Battisti, D. S., and Golubic, S.: Southward movement of the Pacific intertropical convergence zone AD 1400–1850, *Nat. Geosci.*, 2, 519–525, doi:10.1038/ngeo554, 2009. 5552

Saenger, C., Came, R. E., Oppo, D. W., Keigwin, L. D., and Cohen, A. L.: Regional climate variability in the western subtropical North Atlantic during the past two millennia, *Paleoceanography*, 26, 1–12, doi:10.1029/2010PA002038, 2011. 5597

Shin, S. I., Sardeshmukh, P. D., Webb, R. S., Oglesby, R. J., and Barsugli, J. J.: Understanding the mid-Holocene climate, *J. Climate*, 19, 2801–2817, doi:10.1175/JCLI3733.1, 2006. 5552

Smerdon, J. E.: Climate models as a test bed for climate reconstruction methods: pseudoproxy experiments, *Wiley Interdiscip. Rev. Clim. Chang.*, 3, 63–77, doi:10.1002/wcc.149, 2012. 5556, 5557, 5568, 5574, 5575

Stahle, D. S., D'Arrigo, R. D., Krusic, P. J., Cleaveland, M. K., Cook, E. R., Allan, R. J., Cole, J. E., Dunbar, R. B., Therrell, M. D., Gay, D. A., Moore, M. D., Stokes, M. A., Burns, B. T., Villanueva-Diaz, J., and Thompson, L. G.: Experimental Dendroclimatic Reconstruction of the Southern Oscillation, *B. Am. Meteorol. Soc.*, 79, 2137–2152, doi:10.1175/1520-0477(1998)079<2137:EDROTS>2.0.CO;2, 1998. 5565, 5573

Stahle, D. W., Diaz, J. V., Burnette, D. J., Paredes, J. C., Heim, R. R., Fye, F. K., Soto, R. A., Therrell, M. D., and Cleaveland, M. K.: Major mesoamerican droughts of the past millennium, *Geophys. Res. Lett.*, 38, 2–5, doi:10.1029/2010GL046472, 2011. 5593

Stansell, N. D., Steinman, B. A., Abbott, M. B., Rubinov, M., and Roman-Lacayo, M.: Lacustrine stable isotope record of precipitation changes in Nicaragua during the Little Ice Age and Medieval Climate Anomaly, *Geology*, 41, 151–154, doi:10.1130/G33736.1, 2013. 5568, 5593

Steinman, B. A., Abbott, M. B., Mann, M. E., Stansell, N. D., and Finney, B. P.: 1500 year quantitative reconstruction of winter precipitation in the Pacific Northwest, *P. Natl. Acad. Sci. USA*, 109, 11619–11623, doi:10.1073/pnas.1201083109, 2012. 5568, 5593

Stott, L., Poulsen, C., Lund, S., and Thunell, R.: Super ENSO and global climate oscillations at millennial time scales, *Science*, 297, 222–226, doi:10.1126/science.1071627, 2002. 5597

Stott, L., Cannariato, K., Thunell, R., Haug, G. H., Koutavas, A., and Lund, S.: Decline of surface temperature and salinity in the western tropical Pacific Ocean in the Holocene epoch, *Nature*, 431, 56–59, doi:10.1038/nature02903, 2004. 5566

ENSO reconstructions

L. M. K. Henke et al.

Title Page

Abstract

Introduction

Conclusions

References

Tables

Figures



Back

Close

Full Screen / Esc

Printer-friendly Version

Interactive Discussion



- Sturm, C., Zhang, Q., and Noone, D.: An introduction to stable water isotopes in climate models: benefits of forward proxy modelling for paleoclimatology, *Clim. Past*, 6, 115–129, doi:10.5194/cp-6-115-2010, 2010. 5568
- Sundqvist, H. S., Holmgren, K., Fohlmeister, J., Zhang, Q., Matthews, M. B., Spötl, C., and Körnich, H.: Evidence of a large cooling between 1690 and 1740 AD in southern Africa, *Sci. Rep.*, 3, 1–6, doi:10.1038/srep01767, 2013. 5597
- Tan, L., Cai, Y., Cheng, H., An, Z., and Edwards, R. L.: Summer monsoon precipitation variations in central China over the past 750 years derived from a high-resolution absolute-dated stalagmite, *Palaeogeogr. Palaeoclimatol.*, 280, 432–439, doi:10.1016/j.palaeo.2009.06.030, 2009. 5593
- Thompson, D. M., Ault, T. R., Evans, M. N., Cole, J. E., and Emile-Geay, J.: Comparison of observed and simulated tropical climate trends using a forward model of coral $\delta^{18}\text{O}$, *Geophys. Res. Lett.*, 38, 1–6, doi:10.1029/2011GL048224, 2011. 5568
- Thompson, L. G., Mosley-Thompson, E., Davis, M. E., Zagorodnov, V. S., Howat, I. M., Mikhalenko, V. N., and Lin, P.-N.: Annually resolved ice core records of tropical climate variability over the past ~1800 years, *Science*, 340, 945–950, doi:10.1126/science.1234210, 2013. 5597
- Tierney, J. E., Oppo, D. W., Rosenthal, Y., Russell, J. M., and Linsley, B. K.: Coordinated hydrological regimes in the Indo-Pacific region during the past two millennia, *Paleoceanography*, 25, 1–7, doi:10.1029/2009PA001871, 2010. 5552, 5565
- Tierney, J. E., Lewis, S. C., Cook, B. I., LeGrande, A. N., and Schmidt, G. A.: Model, proxy and isotopic perspectives on the East African Humid Period, *Earth Planet. Sc. Lett.*, 307, 103–112, doi:10.1016/j.epsl.2011.04.038, 2011. 5568
- Tingley, M. P., Craigmile, P. F., Haran, M., Li, B., Mannshardt, E., and Rajaratnam, B.: Piecing together the past: Statistical insights into paleoclimatic reconstructions, *Quaternary Sci. Rev.*, 35, 1–22, doi:10.1016/j.quascirev.2012.01.012, 2012. 5559
- Tiwari, M., Nagoji, S. S., and Ganeshram, R. S.: Multi-centennial scale SST and Indian summer monsoon precipitation variability since mid-Holocene and its nonlinear response to solar activity, *Holocene*, 25, 1415–1424, doi:10.1177/0959683615585840, 2015. 5597
- Treydte, K. S., Schleser, G. H., Helle, G., Frank, D. C., Winiger, M., Haug, G. H., and Esper, J.: The twentieth century was the wettest period in northern Pakistan over the past millennium, *Nature*, 440, 1179–1182, doi:10.1038/nature04743, 2006. 5593

ENSO reconstructions

L. M. K. Henke et al.

Title Page

Abstract

Introduction

Conclusions

References

Tables

Figures



Back

Close

Full Screen / Esc

Printer-friendly Version

Interactive Discussion



Trouet, V., Esper, J., Graham, N. E., Baker, A., Scourse, J. D., and Frank, D. C.: Persistent positive North Atlantic oscillation mode dominated the Medieval Climate Anomaly, *Science*, 324, 78–80, doi:10.1126/science.1166349, 2009. 5552

Trouet, V., Scourse, J. D., and Raible, C. C.: North Atlantic storminess and Atlantic meridional overturning circulation during the last millennium: reconciling contradictory proxy records of NAO variability, *Global Planet. Change*, 84–85, 48–55, doi:10.1016/j.gloplacha.2011.10.003, 2012. 5551, 5552

van Oldenborgh, G. J., Philip, S. Y., and Collins, M: El Niño in a changing climate: a multi-model study, *Ocean Sci.*, 1, 81–95, doi:10.5194/os-1-81-2005, 2005. 5551

Vecchi, G. A., and Wittenberg, A. T.: El Niño and our future climate: where do we stand?, *Wiley Interdiscip. Rev. Clim. Chang.*, 1, 260–270, doi:10.1002/wcc.33, 2010. 5551

Wang, H. J., Zhang, R. H., Cole, J. E., and Chavez, F.: El Niño and the related phenomenon Southern Oscillation (ENSO): the largest signal in interannual climate variation, *P. Natl. Acad. Sci. USA*, 96, 11071–11072, doi:10.1073/pnas.96.20.11071, 1999. 5551

Wang, J., Emile-Geay, J., Guillot, D., Smerdon, J. E., and Rajaratnam, B.: Evaluating climate field reconstruction techniques using improved emulations of real-world conditions, *Clim. Past*, 10, 1–19, doi:10.5194/cp-10-1-2014, 2014. 5559, 5567

Wanner, H., Beer, J., Bütikofer, J., Crowley, T. J., Cubasch, U., Flückiger, J., Goosse, H., Grosjean, M., Joos, F., Kaplan, J. O., Küttel, M., Müller, S. A., Prentice, I. C., Solomina, O., Stocker, T. F., Tarasov, P., Wagner, M., and Widmann, M.: Mid- to Late Holocene climate change: an overview, *Quaternary Sci. Rev.*, 27, 1791–1828, doi:10.1016/j.quascirev.2008.06.013, 2008. 5552

Wilson, R., Cook, E. R., D'Arrigo, R. D., Riedwyl, N., Evans, M. N., Tudhope, A. W., and Allan, R.: Reconstructing ENSO: the influence of method, proxy data, climate forcing and teleconnections, *J. Quaternary Sci.*, 25, 62–78, doi:10.1002/jqs.1297, 2010. 5564, 5572

Yan, H., Sun, L., Oppo, D. W., Wang, Y., Liu, Z., Xie, Z., Liu, X., and Cheng, W.: South China Sea hydrological changes and Pacific Walker Circulation variations over the last millennium, *Nat. Commun.*, 2, 293, doi:10.1038/ncomms1297, 2011a. 5552, 5553, 5565

Yan, H., Sun, L., Wang, Y., Huang, W., Qiu, S., and Yang, C.: A record of the Southern Oscillation Index for the past 2000 years from precipitation proxies, *Nat. Geosci.*, 4, 611–614, doi:10.1038/ngeo1231, 2011b. 5552, 5565, 5593

Yang, B., Qin, C., Wang, J., He, M., Melvin, T. M., Osborn, T. J., and Briffa, K. R.: A 3500-year tree-ring record of annual precipitation on the northeastern Tibetan Plateau, P. Natl. Acad. Sci. USA, 111, 2903–2908, doi:10.1073/pnas.1319238111, 2014. 5593

5 Yi, L., Yu, H., Ge, J., Lai, Z., Xu, X., Qin, L., and Peng, S.: Reconstructions of annual summer precipitation and temperature in north-central China since 1470 AD based on drought/flood index and tree-ring records, Climate Change, 110, 469–498, doi:10.1007/s10584-011-0052-6, 2012. 5593

CPD

11, 5549–5604, 2015

ENSO reconstructions

L. M. K. Henke et al.

Title Page

Abstract

Introduction

Conclusions

References

Tables

Figures



Back

Close

Full Screen / Esc

Printer-friendly Version

Interactive Discussion



Table 1. Precipitation proxy details. “Res” is proxy resolution, rounded to the nearest integer; sub-annual proxies are listed as having a 1 year resolution. “Dating” refers to dating error. “Included?” indicates whether the proxy contributed to the final ENSO reconstruction; if not, the reason for exclusion is listed (“Dating error” and “Length” are a priori conditions which the proxies failed to meet. “AOI” indicates it passed pre-processing screening, but was not selected during the add-one-in process).

Reference	Proxy	Start	End	Lon	Lat	Res	Dating	Included?
Anchukaitis and Evans (2010)	tree ring	50	-53	274.7	10.2	1	2	No; Length
Anderson (2011)	lake	10 290	-58	252.7	39.8	100	83	No; Dating error
Asmerom et al. (2007)	speleothem	12 087	-15	254.8	32.1	17	1108	No; Dating error
Bale et al. (2011)	tree ring	865	-55	241.8	37.5	1	1	Yes
Bird et al. (2011)	lake	11 142	-57	283.9	-10.7	20	295	No; Dating error
Bonnefille and Chalil (2000)	peat pollen	40 500	0	356.3	29.7	100	200	No; Dating error
Buckley et al. (2002)	tree ring	920	-58	106.3	11.6	1	1	Yes
Christie et al. (2011)	tree ring	604	-52	290	-37.5	1	1	Yes
Cloveland et al. (2003)	tree ring	564	-43	105.8	25.4	1	1	Yes
Cole et al. (1993)	coral	56	-40	172	1	1	NA	No; Dating error
Conroy et al. (2008)c-n	lake	9191	-54	270.5	-0.9	10	100	No; Dating error
Conroy et al. (2008)clay	lake	9191	-54	270.5	-0.9	10	100	No; Dating error
Conroy et al. (2008)sand	lake	9191	-54	270.5	-0.9	10	100	No; Dating error
Conroy et al. (2008)silt	lake	9191	-54	270.5	-0.9	10	100	No; Dating error
Conroy et al. (2009)	lake	1219	-54	270.5	-0.9	5	100	No; Dating error
Diaz et al. (2002)	tree ring	303	-42	255.2	31.9	1	1	Yes
Faustlich et al. (2013)	tree ring	353	-58	249.9	36	1	1	Yes
Griffin et al. (2013)	tree ring	411	-58	249.5	32.5	1	1	Yes
Haug et al. (2001)fe	marine sediment	14 277	110	294.8	10.7	5	50	Yes
Haug et al. (2001)li	marine sediment	14 277	110	294.8	10.7	5	50	Yes
Hendy et al. (2003)	coral	338	-35	146.6	-18.3	1	1	Yes
Kennett et al. (2012)	speleothem	1989	-54	270.9	16.2	1	19	Yes
Maupin et al. (2014)10fc	speleothem	527	-60	160	-9.5	1	6	Yes
Maupin et al. (2014)5fc	speleothem	70	-26	160	-9.5	1	5	No; Length
Medina-Elizalde et al. (2010)	speleothem	1463	-54	270.5	20.7	2.3	10	Yes
Moy et al. (2002)	lake	15 117	-27	280.8	2.8	100	60	Yes
Nelson et al. (2011)	lake	6000	101	240.4	48.5	5	100	No; Dating error
Oppo et al. (2009)d18ow	marine sediment	1925	-5	116.5	-4.5	11	95	No; Dating error
Partin et al. (2007)	speleothem	26 420	0	115	4.3	100	300	No; Dating error
Partin et al. (2013)	speleothem	393	-55	167	-15.5	1	11	Yes
Pohl et al. (2003)	tree ring	168	-50	259.5	25.3	1	1	No; Length
Rasbury and Aharon (2006)asm1	speleothem	121	-51	190.2	-19	1	7	No; Length
Rasbury and Aharon (2006)asm2	speleothem	190	-51	190.2	-19	1	5	No; Length
Rasbury and Aharon (2006)asm3	speleothem	76	-51	190.2	-19	1	13	No; Length
Rasbury and Aharon (2006)asm4	speleothem	67	22	190.2	-19	1	13	No; Length
Reuter et al. (2009)a	speleothem	47	-56	282.8	-6.1	1	9	No; Length
Reuter et al. (2009)d	speleothem	861	43	282.8	-6.1	1	9	Yes
Rodbell (1999)old	lake	15 117	802	280.8	2.8	1	10	Yes
Rodbell (1999)recent	lake	662	-27	280.8	2.8	1	10	Yes
Rocystill et al. (2012)	lake	1290	-59	113.3	-8	55	80	Yes
Russell and Johnson (2007)	lake	1399	-24	29.8	-0.4	3	10	Yes
Stahle et al. (2011)	tree ring	1179	-58	263.7	19.1	1	1	Yes
Stensell et al. (2013)	lake	1609	-54	274.1	11.9	5	10	Yes
Steinman et al. (2012)castor	lake	1450	-50	240.4	48.5	5	100	No; Dating error
Tan et al. (2009)	speleothem	701	-33	106.3	33.1	3	8	Yes
Treydte et al. (2006)	tree ring	950	-48	74.9	36.6	1	1	No; AOI
Yan et al. (2011b)jd2	lake	926	-46	112.7	16.7	15	70	No; Dating error
Yan et al. (2011b)jd4	lake	926	-46	112.7	16.7	20	70	No; Dating error
Yan et al. (2011b)jd6	lake	926	-53	112.7	16.7	10	70	No; Dating error
Yang et al. (2014)	tree ring	3450	-61	98.5	37.9	1	1	No; AOI
Yi et al. (2012)a	tree ring	350	-50	110	34.5	1	1	No; AOI
Yi et al. (2012)b	tree ring	350	-50	112	39.5	1	1	No; AOI

Title Page

Abstract

Introduction

Conclusions

References

Tables

Figures



Back

Close

Full Screen / Esc

Printer-friendly Version

Interactive Discussion



ENSO reconstructions

L. M. K. Henke et al.

Title Page

Abstract

Introduction

Conclusions

References

Tables

Figures



Back

Close

Full Screen / Esc

Printer-friendly Version

Interactive Discussion



Table 2. Temperature proxy details. “Res” is proxy resolution, rounded to the nearest integer; sub-annual proxies are listed as having a 1 year resolution. “Dating” refers to dating error. “Included?” indicates whether the proxy contributed to the final ENSO reconstruction; if not, the reason for exclusion is listed (“Dating error” and “Length” are a priori conditions which the proxies failed to meet. “AOI” indicates it passed pre-processing screening, but was not selected during the add-one-in process).

Reference	Proxy	Start	End	Lon	Lat	Res	Dating	Included?
Abram et al. (2009)mentawai	coral	7244	-51	98.9	-1.4	9	15	No; AOI
Abram et al. (2009)png	coral	7550	25	144.7	-3.6	18	89	No; Dating error
ar018	tree ring	300	-29	265.6	34.7	1	1	Yes
ar024	tree ring	225	-29	265.6	36.1	1	1	Yes
ar030	tree ring	214	-29	266.5	34.5	1	1	Yes
ar042	tree ring	428	-29	268.3	34.6	1	1	Yes
ar048	tree ring	533	-29	269.1	35.9	1	1	Yes
ar050	tree ring	931	-30	268.7	35.2	1	1	Yes
ar055	tree ring	591	-42	266.7	36.1	1	1	Yes
ar056	tree ring	280	-42	266.7	36.1	1	1	Yes
ar057	tree ring	330	-43	266.8	36.1	1	1	Yes
ar058	tree ring	271	-42	265.9	36.1	1	1	Yes
ar060	tree ring	313	-43	267.8	36.3	1	1	Yes
ar061	tree ring	258	-43	267.1	36.9	1	1	Yes
ar064	tree ring	292	-41	265.8	34.3	1	1	Yes
ar072	tree ring	325	-41	266	35.8	1	1	Yes
aust002	tree ring	384	-21	11	46.9	1	1	Yes
az080	tree ring	352	-21	250.7	36.1	1	1	Yes
az081	tree ring	349	-21	250.6	36.1	1	1	Yes
az082	tree ring	574	-22	250.6	36.1	1	1	Yes
az084	tree ring	480	-21	249.5	36.2	1	1	Yes
az086	tree ring	585	-21	249.3	36.8	1	1	Yes
az089	tree ring	354	-22	250.2	34.3	1	1	Yes
az091	tree ring	261	-22	248.4	35.6	1	1	Yes
az098	tree ring	302	-22	248.2	35.5	1	1	Yes
az099	tree ring	263	-23	250.1	34.5	1	1	Yes
az102	tree ring	460	-22	249.5	36.7	1	1	Yes
az104	tree ring	356	-21	246.3	36.8	1	1	Yes
az106	tree ring	502	-25	247.9	35.8	1	1	Yes
az109	tree ring	352	-21	247	35	1	1	Yes
az127	tree ring	369	-26	247.8	36.7	1	1	Yes
az129	tree ring	468	-26	247.9	36.6	1	1	Yes
az135	tree ring	381	-21	246.1	35.1	1	1	Yes
az143	tree ring	307	-22	246.9	36	1	1	Yes
az144	tree ring	469	-25	248	36.8	1	1	Yes
az505	tree ring	257	-25	248	36.4	1	1	Yes
az510	tree ring	1402	-33	248.3	35.5	1	1	Yes
az527	tree ring	320	-36	249.2	34.3	1	1	Yes
az542	tree ring	320	-36	250.1	34.3	1	1	Yes
Barron (2003)	marine sediment	15 804	158	235.1	41.7	100	910	No; Dating error
Boiseau et al. (1999)	coral	98	-41	210.2	-17.5	1	1	No; Length
ca051	tree ring	1992	-20	243.2	34.1	1	1	Yes
ca066	tree ring	479	-30	239.4	40.2	1	1	Yes
ca067	tree ring	466	-30	239.4	40.2	1	1	Yes
ca089	tree ring	445	-31	241.7	35.4	1	1	Yes
ca092	tree ring	516	-31	241.1	36.7	1	1	Yes
ca094	tree ring	422	-31	241.6	35.5	1	1	Yes
ca514	tree ring	343	-31	241.8	36	1	1	Yes
ca528	tree ring	1052	-37	241.6	36.8	1	1	Yes
ca529	tree ring	1251	-37	241.4	36.5	1	1	Yes

Table 2. Continued.

Reference	Proxy	Start	End	Lon	Lat	Res	Dating	Included?
ca530	tree ring	1033	-37	241.8	36.5	1	1	Yes
ca531	tree ring	923	-37	241.8	36.8	1	1	Yes
ca532	tree ring	900	-37	241.4	36.5	1	1	Yes
ca536	tree ring	296	-38	242.7	34.3	1	1	Yes
ca544	tree ring	243	-38	242.9	34.2	1	1	Yes
ca546	tree ring	209	-38	242.9	34.2	1	1	Yes
ca547	tree ring	266	-38	243	34.2	1	1	Yes
ca552	tree ring	322	-38	243	34.1	1	1	Yes
ca555	tree ring	773	-38	237.1	40	1	1	Yes
ca609	tree ring	390	-45	243.2	34.1	1	1	Yes
ca612	tree ring	480	-43	240.6	34.7	1	1	Yes
ca619	tree ring	587	-54	238.2	40.3	1	1	Yes
ca621	tree ring	365	-53	241.3	35.5	1	1	Yes
ca625	tree ring	440	-53	239	37.1	1	1	Yes
ca626	tree ring	373	-53	238.8	36.5	1	1	Yes
ca628	tree ring	500	-48	239.4	40.2	1	1	Yes
co066	tree ring	493	-28	251.5	37.6	1	1	Yes
co067	tree ring	680	-28	251.5	37.6	1	1	Yes
co511	tree ring	781	-39	254.4	40	1	1	Yes
co526	tree ring	300	-30	254.5	40.4	1	1	Yes
co532	tree ring	310	-37	254.4	40.4	1	1	Yes
co533	tree ring	400	-37	254.7	39.9	1	1	Yes
co538	tree ring	280	-37	254.9	40.5	1	1	Yes
co542	tree ring	260	-37	254.7	40.2	1	1	Yes
co543	tree ring	380	-37	254.2	40.4	1	1	Yes
co544	tree ring	520	-37	254.3	40.1	1	1	Yes
co545	tree ring	620	-37	254.5	40.1	1	1	Yes
co547	tree ring	880	-37	254.3	40.4	1	1	Yes
co548	tree ring	300	-38	255.1	38.6	1	1	Yes
co549	tree ring	440	-37	254.3	40.4	1	1	Yes
co550	tree ring	260	-37	254.8	40.4	1	1	Yes
co551	tree ring	200	-37	254.6	40.1	1	1	Yes
co563	tree ring	252	-51	254.4	40.4	1	1	Yes
co568	tree ring	322	-48	256.8	37.2	1	1	Yes
co569	tree ring	486	-47	256.4	37.1	1	1	Yes
co572	tree ring	1056	-48	254.5	40.3	1	1	Yes
co579	tree ring	630	-52	253.5	40	1	1	Yes
co581	tree ring	411	-50	253.2	40.8	1	1	Yes
Cobb et al. (2003)full	coral	1022	-48	197.9	5.9	1	0.25	Yes
Cook et al. (2000)	tree ring	3550	-41	145.5	-41.8	1	1	Yes
Cronin et al. (2003)	sediment	2134	-45	283.7	38.3	8	160	No; Dating error
Damassa et al. (2006)c17th	coral	328	228	39.5	-8	1	5	Yes
Damassa et al. (2006)c20th	coral	53	-48	39.5	-8	1	5	No; Length
DeLong et al. (2012)	coral	301	-50	166.5	-22.5	1	1	Yes
Felis et al. (2010)srca	coral	77	-44	142.2	27.1	1	1	No; Length
Felis et al. (2010)uca	coral	77	-44	142.2	27.1	1	1	No; Length
ia003	tree ring	235	-31	268	40.7	1	1	Yes
id002	tree ring	278	-26	244.1	47.5	1	1	Yes
ii010	tree ring	279	-30	270.2	40	1	1	Yes
ii011	tree ring	276	-30	271.8	39.4	1	1	Yes
ii013	tree ring	295	-31	271	37.5	1	1	Yes
ii014	tree ring	298	-31	270.8	37.6	1	1	Yes
indi002	tree ring	346	-30	74.3	35.1	1	1	Yes
indi006	tree ring	296	-31	75.5	34.6	1	1	Yes
ital023	tree ring	476	-40	12.1	46.6	1	1	Yes
Keigwin (1996)	marine sediment	3125	25	302.4	33.7	50	150	No; Dating error
Kellerhals et al. (2010)	ice core	1595	-45	292.2	-16.6	10	20	Yes
Khider et al. (2014)sst	marine sediment	9960	199	125.8	6.5	30	530	No; Dating error

Title Page

Abstract

Introduction

Conclusions

References

Tables

Figures



Back

Close

Full Screen / Esc

Printer-friendly Version

Interactive Discussion



Table 2. Continued.

Reference	Proxy	Start	End	Lon	Lat	Res	Dating	Included?
ks007	tree ring	212	-29	264.1	37.6	1	1	Yes
ky003	tree ring	290	-32	277	37.1	1	1	Yes
Marchitto et al. (2010)	marine sediment	13 812	832	247.3	25.2	50	50	Yes
me019	tree ring	253	-31	291.7	45.5	1	1	Yes
mi009	tree ring	440	-33	275.1	46.5	1	1	Yes
mo003	tree ring	257	-31	268.5	37.1	1	1	Yes
mo005	tree ring	242	-32	269.5	37.5	1	1	Yes
mo018	tree ring	226	-29	266.2	36.6	1	1	Yes
mo033	tree ring	254	-42	267.2	36.7	1	1	Yes
mo036	tree ring	261	-29	266.2	36.6	1	1	Yes
mo037	tree ring	765	-42	269.5	36.6	1	1	Yes
mo038	tree ring	397	-42	267.5	37.2	1	1	Yes
mo039	tree ring	286	-42	268.1	37.5	1	1	Yes
mo040	tree ring	257	-43	268.8	37.1	1	1	Yes
mo043	tree ring	812	-40	268.5	37.1	1	1	Yes
morc002	tree ring	318	-34	355.2	35	1	1	Yes
nc002	tree ring	392	-33	276.6	35.6	1	1	Yes
nc003	tree ring	390	-33	278.2	36.1	1	1	Yes
nc006	tree ring	273	-33	276.8	35.1	1	1	Yes
nc007	tree ring	333	-27	278.1	35.9	1	1	Yes
nc009	tree ring	426	-34	283.4	36.5	1	1	Yes
nj001	tree ring	330	-32	285.4	40.5	1	1	Yes
nj002	tree ring	276	-32	285.4	40.5	1	1	Yes
nm021	tree ring	395	-21	252.2	37	1	1	Yes
nm023	tree ring	375	-21	252.2	37	1	1	Yes
nm024	tree ring	307	-21	252.7	36.7	1	1	Yes
nm025	tree ring	569	-22	251.9	35.6	1	1	Yes
nm026	tree ring	588	-22	253.5	36.4	1	1	Yes
nm031	tree ring	472	-22	251.5	35.4	1	1	Yes
nm033	tree ring	414	-22	251.7	35	1	1	Yes
nm034	tree ring	288	-22	252.2	34.9	1	1	Yes
nm038	tree ring	394	-22	254.3	35.5	1	1	Yes
nm040	tree ring	371	-22	254.4	35.5	1	1	Yes
nm047	tree ring	310	-24	257	36.8	1	1	Yes
nm051	tree ring	263	-26	252.8	35.6	1	1	Yes
nm053	tree ring	321	-26	252.4	35.9	1	1	Yes
nm055	tree ring	356	-21	252.7	36.7	1	1	Yes
nm118	tree ring	386	-32	254.4	35.1	1	1	Yes
nm500	tree ring	242	-22	254.3	36.1	1	1	Yes
nm501	tree ring	223	-22	253.7	35.8	1	1	Yes
nm529	tree ring	298	-27	251.2	36	1	1	Yes
nm548	tree ring	358	-31	254.5	36.7	1	1	Yes
nm549	tree ring	311	-37	254.5	36.7	1	1	Yes
nm550	tree ring	418	-36	253.3	35.9	1	1	Yes
nm551	tree ring	250	-31	254.6	36.3	1	1	Yes
nm552	tree ring	369	-31	254.6	36.3	1	1	Yes
nm554	tree ring	260	-36	254.5	36.1	1	1	Yes
nm555	tree ring	346	-36	253.4	35.8	1	1	Yes
nm556	tree ring	378	-36	253.4	35.8	1	1	Yes
nm557	tree ring	395	-36	254.4	36.2	1	1	Yes
nm558	tree ring	297	-37	253.4	35.8	1	1	Yes
nm559	tree ring	559	-37	254.6	36.7	1	1	Yes
nm560	tree ring	1113	-39	254.5	36.7	1	1	Yes
nm575	tree ring	238	-48	256	36.8	1	1	Yes
nm576	tree ring	324	-48	256.1	36.8	1	1	Yes
nm577	tree ring	355	-48	255.7	36.1	1	1	Yes
nv048	tree ring	447	-28	244.5	40.2	1	1	Yes
nv506	tree ring	345	-27	244.8	36.7	1	1	Yes
nv507	tree ring	485	-26	245.1	39.4	1	1	Yes

Title Page

Abstract

Introduction

Conclusions

References

Tables

Figures



Back

Close

Full Screen / Esc

Printer-friendly Version

Interactive Discussion



Table 2. Continued.

Reference	Proxy	Start	End	Lon	Lat	Res	Dating	Included?
nv509	tree ring	399	-26	245.3	39.4	1	1	Yes
nv510	tree ring	1150	-34	244.3	36.3	1	1	Yes
nv512	tree ring	1630	-35	244.5	40.2	1	1	Yes
nv513	tree ring	1125	-33	245.7	38.9	1	1	Yes
nv514	tree ring	1648	-35	245.2	40.6	1	1	Yes
nv516	tree ring	1950	-34	245.8	38.9	1	1	Yes
nv517	tree ring	1630	-34	244.3	36.3	1	1	Yes
oh003	tree ring	288	-35	275.6	39.9	1	1	Yes
oh006	tree ring	325	-48	279	40	1	1	Yes
ok001	tree ring	275	-29	265.3	36.7	1	1	Yes
ok004	tree ring	213	-29	263.6	36.7	1	1	Yes
ok007	tree ring	339	-45	263.8	36.2	1	1	Yes
ok013	tree ring	270	-29	261.6	35.6	1	1	Yes
ok016	tree ring	205	-29	264.4	35.1	1	1	Yes
ok019	tree ring	326	-29	265.4	34.3	1	1	Yes
ok025	tree ring	259	-45	262.3	34.1	1	1	Yes
ok028	tree ring	264	-29	261.4	34.7	1	1	Yes
ok031	tree ring	265	-32	265.4	34.3	1	1	Yes
Oppo et al. (2009)sst	marine sediment	1925	-5	118.5	-4.5	11	95	No; Dating error
or040	tree ring	275	-41	242	45.8	1	1	Yes
pa001	tree ring	341	-31	282.3	40.7	1	1	Yes
pa005	tree ring	327	-31	280.3	39.8	1	1	Yes
pa007	tree ring	415	-31	282.4	40.2	1	1	Yes
pa009	tree ring	319	-31	283.6	39.9	1	1	Yes
pa012	tree ring	338	-31	281.5	39.8	1	1	Yes
Powers et al. (2011)	lake sediment	667	-46	34.3	-10	41	50	No; AOI
Quinn et al. (1998)	coral	292	-43	166.5	-22.5	1	1	Yes
Richey et al. (2009)fsk	marine sediment	702	-50	267.8	27.6	19	35	Yes
Richey et al. (2009)garrison	marine sediment	529	-50	266.1	26.7	33	45	Yes
Saenger et al. (2011)ggc	marine sediment	1500	100	283.7	32.8	100	45	Yes
Saenger et al. (2011)mc	marine sediment	1700	100	283.7	32.8	100	40	Yes
spai009	tree ring	262	-38	357.9	40.4	1	1	Yes
spai011	tree ring	465	-38	357.9	40.2	1	1	Yes
spai013	tree ring	265	-42	0.1	40	1	1	Yes
spai016	tree ring	283	-38	355.2	40.5	1	1	Yes
spai018	tree ring	263	-39	355.1	40.4	1	1	Yes
spai019	tree ring	427	-38	356	40.8	1	1	Yes
spai029	tree ring	239	-33	358.1	40.2	1	1	Yes
spai036	tree ring	201	-33	356	40.8	1	1	Yes
spai037	tree ring	289	-35	356.2	40.8	1	1	Yes
spai038	tree ring	351	-34	356.1	40.8	1	1	Yes
spai041	tree ring	269	-35	0.7	40.3	1	1	Yes
spai045	tree ring	312	-35	358.1	40.3	1	1	Yes
spai046	tree ring	306	-35	358.1	40.3	1	1	Yes
Stott et al. (2002)gruber	marine sediment	67 592	5	125.8	6.3	100	86	No; Dating error
Stott et al. (2002)gsaccullifer	marine sediment	67 592	5	125.8	6.3	100	86	No; Dating error
Sundqvist et al. (2013)	speleothem	315	-43	29.2	-24	1	2.5	Yes
Thompson et al. (2013)nd	ice core	945	-45	289.2	-13.9	10	10	Yes
Thompson et al. (2013)sd	ice core	1724	-59	289.2	-13.9	1	10	Yes
Tiwari et al. (2015)	marine sediment	4772	154	74.1	12.5	62	45	Yes
tin008	tree ring	317	-30	275.9	36.2	1	1	Yes
turk001	tree ring	658	-51	31.1	40	1	1	Yes
turk005	tree ring	580	-38	29.9	36.7	1	1	Yes
turk006	tree ring	590	-38	29.9	36.7	1	1	Yes

Title Page

Abstract

Introduction

Conclusions

References

Tables

Figures



Back

Close

Full Screen / Esc

Printer-friendly Version

Interactive Discussion



ENSO reconstructions

L. M. K. Henke et al.

Table 2. Continued.

Reference	Proxy	Start	End	Lon	Lat	Res	Dating	Included?
ut013	tree ring	517	-21	250	40.8	1	1	Yes
ut018	tree ring	461	-22	250.8	38.5	1	1	Yes
ut020	tree ring	505	-21	250.1	37.5	1	1	Yes
ut021	tree ring	385	-21	249.2	37	1	1	Yes
ut023	tree ring	603	-22	250	37.6	1	1	Yes
ut024	tree ring	674	-20	250.3	37.6	1	1	Yes
ut501	tree ring	315	-21	250.1	40.6	1	1	Yes
va008	tree ring	290	-28	280.7	38.3	1	1	Yes
va009	tree ring	363	-32	280.6	37.6	1	1	Yes
va010	tree ring	419	-32	280.5	37.5	1	1	Yes
va012	tree ring	305	-32	278.3	36.7	1	1	Yes
Hengstum et al. (2015)whc4	marine sediment	2792	-56	295.3	32.3	30	35	Yes
wa048	tree ring	664	-29	238.4	46.9	1	1	Yes
wa056	tree ring	691	-29	238.5	47.4	1	1	Yes
wa057	tree ring	520	-30	239	47.5	1	1	Yes
wa058	tree ring	533	-30	236.7	47.5	1	1	Yes
wa063	tree ring	364	-30	238.5	46.9	1	1	Yes
wa065	tree ring	408	-32	239.2	47.5	1	1	Yes
wa085	tree ring	435	-37	238.7	47.4	1	1	Yes
wv002	tree ring	440	-29	280.6	38.9	1	1	Yes

Title Page

Abstract

Introduction

Conclusions

References

Tables

Figures



Back

Close

Full Screen / Esc

Printer-friendly Version

Interactive Discussion



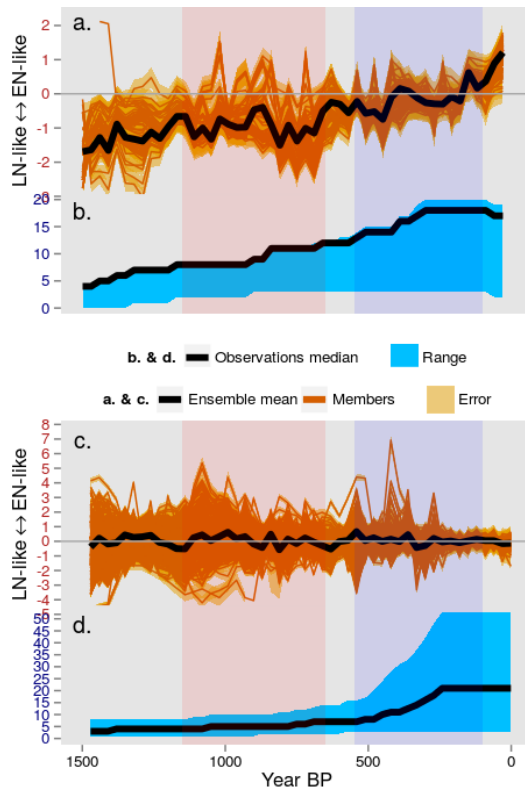


Figure 1. Precipitation and temperature ENSO ensembles. **(a)** 30 year averaged precipitation ENSO reconstruction (black line). Individual network solutions are shown as orange lines, with the uncertainty envelope in orange shading. **(b)** Number of proxies included in the ensemble over time, with the median in black and the range in blue. The pink and purple shaded periods are the MCA and LIA respectively. **(c, d)** are the temperature versions of **(a, b)** respectively.

Title Page

Abstract

Introduction

Conclusions

References

Tables

Figures



Back

Close

Full Screen / Esc

Printer-friendly Version

Interactive Discussion



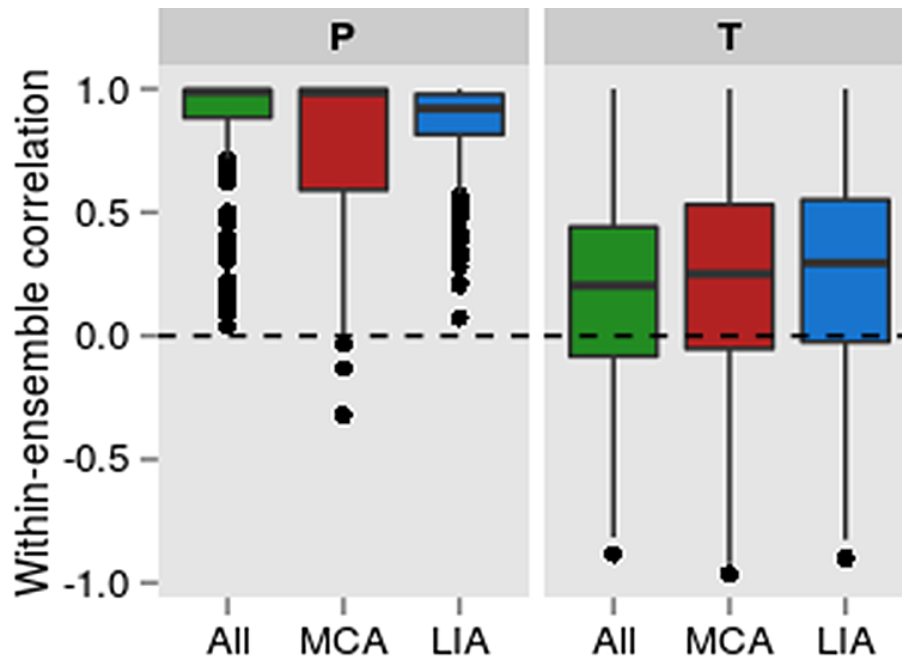


Figure 2. Within-ensemble correlations. Correlations between 1000 pairs randomly chosen from the precipitation and temperature ensembles. Box plots encapsulate the space between the first and third quartile with the median shown as a black line; whiskers indicate the 95 % confidence interval of the median; points are values outside this confidence interval (outliers).

[Title Page](#)

[Abstract](#)

[Introduction](#)

[Conclusions](#)

[References](#)

[Tables](#)

[Figures](#)

[◀](#)

[▶](#)

[◀](#)

[▶](#)

[Back](#)

[Close](#)

[Full Screen / Esc](#)

[Printer-friendly Version](#)

[Interactive Discussion](#)



ENSO reconstructions

L. M. K. Henke et al.

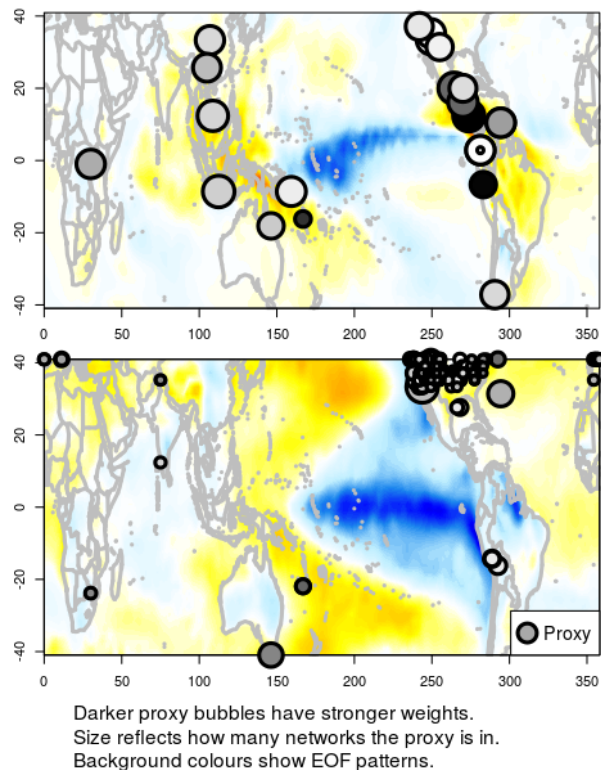


Figure 3. Precipitation EOF with proxy locations. The size of the bubble is indicative of how often the proxy is included in the network ensemble. The colour is related to the proxy weights, such that darker colours are more strongly positive or negative; The relative signs can be gleaned from the EOF pattern.

Title Page

Abstract

Introduction

Conclusions

References

Tables

Figures



Back

Close

Full Screen / Esc

Printer-friendly Version

Interactive Discussion



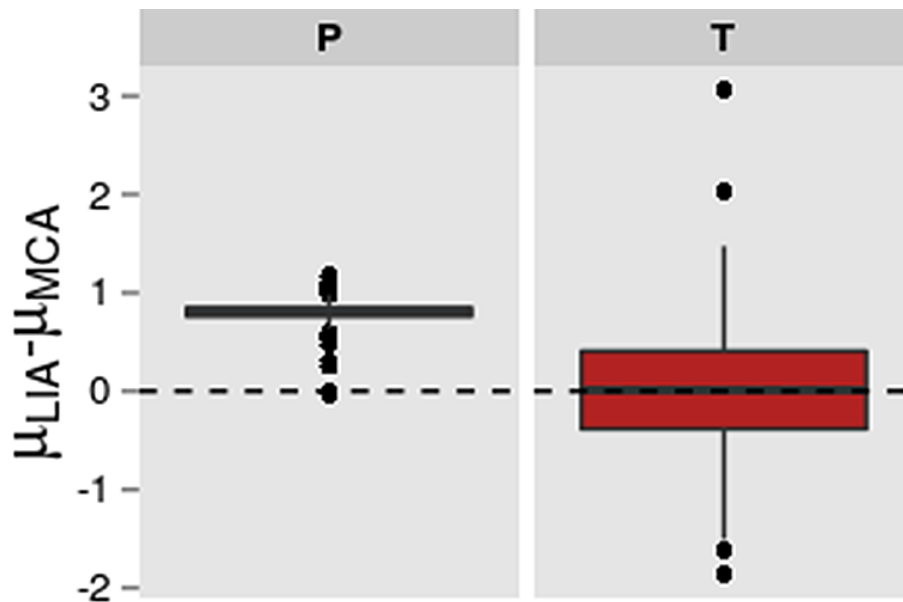


Figure 4. Difference between the means of the MCA and LIA. Difference calculated by subtracting μ_{MCA} from μ_{LIA} for each ensemble member. A positive value indicates LIA is more El Niño-like than MCA. Precipitation is on the left in blue, temperature is on the right in red. See Fig. 2 for explanation of the box plots.

Title Page

Abstract

Introduction

Conclusions

References

Tables

Figures

◀

▶

◀

▶

Back

Close

Full Screen / Esc

Printer-friendly Version

Interactive Discussion



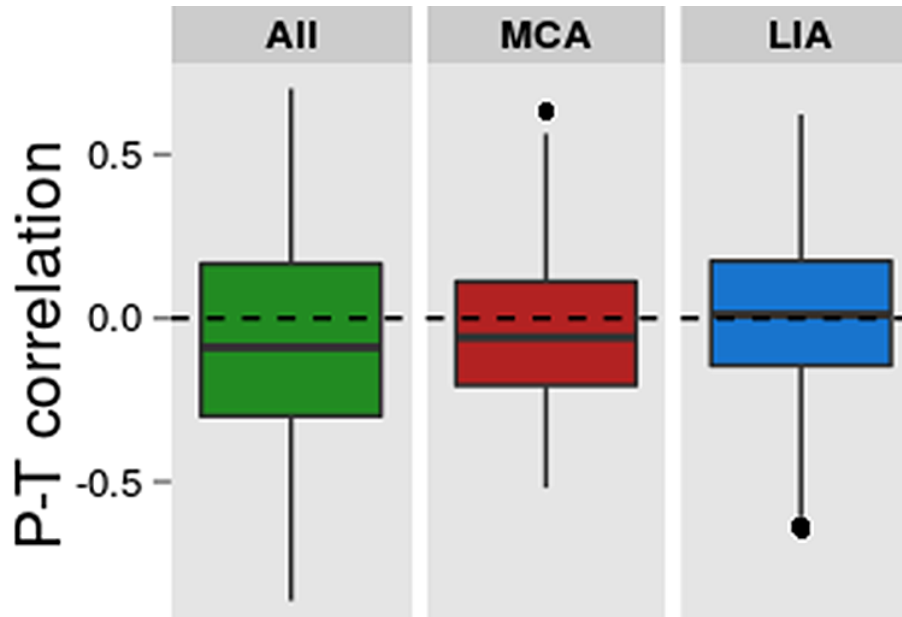


Figure 5. Precipitation – temperature correlations. Correlations between the temperature and precipitation ensemble members based on 1000 randomly chosen pairs. See Fig. 2 for explanation of the box plots.

Title Page

Abstract

Introduction

Conclusions

References

Tables

Figures



Back

Close

Full Screen / Esc

Printer-friendly Version

Interactive Discussion



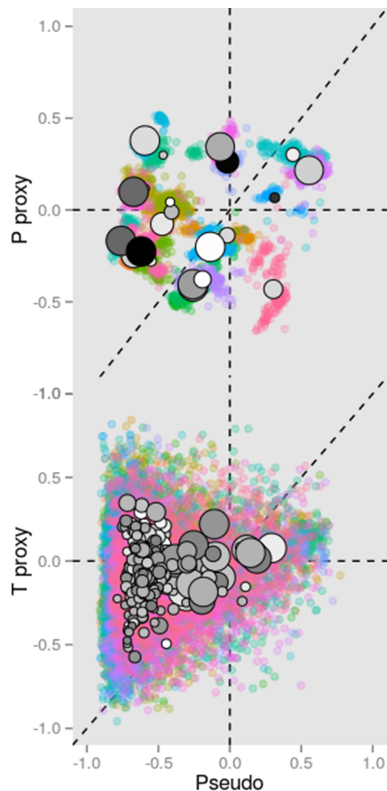


Figure 6. LOO results. LOO results: proxy – ENSO reconstruction correlations in the real world plotted against the reanalysis-derived pseudo world. Proxy records are separated by colour, with a point for each network in which the proxy appears. Dots with black outlines are mean values; size denotes the length of the proxy record and shading is as in Fig. 3.

ENSO reconstructions

L. M. K. Henke et al.

[Title Page](#)

[Abstract](#) | [Introduction](#)

[Conclusions](#) | [References](#)

[Tables](#) | [Figures](#)

[◀](#) | [▶](#)

[◀](#) | [▶](#)

[Back](#) | [Close](#)

[Full Screen / Esc](#)

[Printer-friendly Version](#)

[Interactive Discussion](#)

